Validation strategies for antibodies targeting modified ribonucleotides

Franziska Weichmann[1], Robert Hett[1], Aloys Schepers[2], Taku Ito-Kureha[3], Andrew Flatley[2], Kaouthar Slama[4], Florian D. Hastert[5], Nick Angstmann[6], M. Cristina Cardoso[5], Julian König[7], Stefan Hüttelmaier[8], Christoph Dieterich[9], Stefan Canzar[6], Mark Helm[4], Vigo Heissmeyer[3,10], Regina Feederle[2] & Gunter Meister[1]

[1] Biochemistry Center Regensburg (BZR), Laboratory for RNA Biology, University of Regensburg, Regensburg, Germany

[2] Institute for Diabetes & Obesity, Monoclonal Antibody Core Facility & Research Group, Helmholtz Zentrum München, German Research Center for Environmental Health (GmbH), Ingolstädter Landstr. 1, 85764 Neuherberg, Germany

[3] Institute for Immunology, Biomedical Center of the Ludwig-Maximilians-University München, Grosshaderner Str. 9, 82152 Planegg-Martinsried, Germany

[4] Institute of Pharmacy and Biochemistry, Johannes-Gutenberg-Universität Mainz, Staudingerweg 5, 55128 Mainz, Germany

[5] Cell Biology and Epigenetics, Technische Universität Darmstadt, Schnittspahnstr. 10, 64287 Darmstadt, Germany

[6] Gene Center, Ludwig-Maximilians-University Munich, 81377 Munich, Germany

[7] Institute of Molecular Biology (IMB), Ackermannweg 4, 55128 Mainz, Germany

[8] Institute of Molecular Medicine, Section for Molecular Cell Biology, Faculty of Medicine, Martin Luther University Halle-Wittenberg, Charles Tanford Protein Centre, Kurt-Mothes-Str. 3a, 06120 Halle, Germany

[9] Bioinformatics and Systems Cardiology, Klaus Tschira Institute for Integrative Computational Cardiology and Department of Internal Medicine III, University Hospital Heidelberg, 69120 Heidelberg, Germany

[10] Research Unit Molecular Immune Regulation, Helmholtz Zentrum München, Deutsches Forschungszentrum für Gesundheit und Umwelt (GmbH), Marchioninistr. 25, 81377 Munich, Germany

Correspondence should be addressed to G.M. (gunter.meister@ur.de)

Running Title: Antibodies against base modifications

Keywords: monoclonal antibodies, affinity, m^6A, m^5C, validation, base modifications

Abstract

Chemical modifications are found on almost all RNAs and affect their coding and non-coding functions. The identification of m^6A on mRNA and its important role in gene regulation stimulated the field to investigate whether additional modifications are present on mRNAs. Indeed, modifications including m^1A, m^5C, m^7G, 2'-OMe and Ψ were detected. However, since their abundances are low and tools used for their corroboration are often not well characterized, their physiological relevance remains largely elusive. Antibodies targeting modified nucleotides are often used but have limitations such as low affinity or specificity. Moreover, they are not always well characterized and due to the low abundance of the modification, particularly on mRNAs, generated datasets might resemble noise rather than specific modification patterns. Therefore, it is critical that the affinity and specificity is rigorously tested using complementary approaches. Here, we provide an experimental toolbox that allow for testing antibody performance prior to their use.

Introduction

RNA molecules are composed of nucleotides carrying the four bases Adenine (A), Guanine (G), Cytosine (C) and Uracil (U). Soon after the discovery of RNAs with non-coding functions such as transfer RNAs (tRNAs) or ribosomal RNAs (rRNAs), it became evident that RNAs can be heavily modified and these modifications are important for their structures and functions (Littlefield and Dunn 1958; Bergquist and Matthews 1962). Bases can be chemically modified to gain or lose specific biophysical properties. Such modifications may, for example, lead to changes in RNA base pairing or RNA folding (Motorin and Helm 2011; Polikanov et al. 2015). In addition, some modifications could generate binding platforms for specialized RNA

binding proteins (RBPs). A prominent example for modified bases is pseudouridine (Ψ), which is present in rRNA, tRNA and also mRNA (Zhao et al. 2017). The modification reactions are catalyzed by specialized RNA-protein complexes (RNPs) containing box H/ACA small nucleolar RNAs (snoRNAs) and the associated catalytic subunit dyskerin (snoRNPs) (Matera et al. 2007).

The recent developments in RNA sequencing technologies revealed that modifications are widespread and found in almost all RNAs including mRNAs (Helm and Motorin 2017). An example for an abundant modification found in mRNAs is N6-methyl-Adenosine (m^6A) (Dominissini et al. 2012; Meyer et al. 2012). This modification is generated on mRNAs by the METTL3-METTL14 enzyme complex (Batista et al. 2014; Liu et al. 2014; Meyer and Jaffrey 2017). A multitude of different m^6A methylation patterns have been reported and thus many cellular functions are associated with this modification (Fu et al. 2014; Maity and Das 2016). For example, m^6A is enriched around stop codons, on 3' UTRs and in large exons (Ke et al. 2015; Yue et al. 2015). In the nucleus, m^6A modification accelerates turnover of modified transcripts but seems to be dispensable for splicing (Ke et al. 2017). In contrast, it has been reported that hnRNPG binds RNA polymerase II and m^6A modifications on nascent pre-mRNAs leading to changes in splicing patterns (Zhou et al. 2019). In the cytoplasm, m^6A promotes cap-independent translation initiation by direct recruitment of initiation factors (Meyer et al. 2015; Coots et al. 2017; Yang et al. 2017).

In addition to m^6A, a number of other mRNA modifications have been reported. M^1A (N1-methyladenosine) has recently been identified on cytosolic and mitochondrial mRNA but probably at low frequency (Li et al. 2017; Safra et al. 2017). Ψ has been profiled and found that mRNAs also carry this modification (Carlile et al. 2014; Lovejoy et al. 2014; Schwartz et al. 2014; Li et al. 2015). M^5C (5-methylcytosine), a

common modification found on DNA, has been reported on mRNAs as well (Squires et al. 2012; Amort et al. 2017; Legrand et al. 2017) (Huang et al. 2019) and this phenomenon appears to be conserved in Archaea (Edelheit et al. 2013). In addition, non-coding RNAs have also been found to contain m^5C modifications (Hussain et al. 2013; Trixl and Lusser 2019). Most of these m^5C studies utilized bisulfite-sequencing protocols, which are widely used for studying DNA m^5C modifications and found very few to thousands of methylated sites on mRNAs. Other studies used m^5C-specific antibodies to validate bisulfite-sequencing results. However, available antibodies were often selected for DNA specificity and their applicability for single stranded RNA is unclear.

It is likely that the abovementioned examples are more the tip of the iceberg rather than a complete picture of mRNA base modifications. M^6A is among the best-studied mRNA modification to date and this is due to the rather high abundance and the availability of antibodies against this modification. Some of them have been developed a long time ago and proved to be invaluable tools for the analysis of m^6A on mRNA (e.g. (Bringmann and Luhrmann 1987)). Antibodies against other base modifications have been generated but low modification abundance as well as a lack of thorough validation led to rather vague results in RNA-seq experiments (Grozhik et al. 2019; Helm et al. 2019). Thus, a rigorous validation of base-specific antibodies for each individual assay that is applied is a critical prerequisite for the generation of conclusive and trustable data (Feederle and Schepers 2017).

To help solving this fundamental problem, we developed a panel of assays for antibody validation. In addition, we generated our own monoclonal antibodies against m^6A, m^5C, $m_2{}^6A$ (N6, N6-Dimethyladenosine) and Ψ to prove the applicability of our validation and testing pipeline (Erlanger and Beiser 1964). We employed a number of

biochemical and biophysical assays and measurements ranging from K_d and enrichment factor determination to immunofluorescence and FACS analysis. Our study provides a detailed characterization platform for antibodies against base modifications helping to define quality standards for these widely used research tools.

Results

Generation of monoclonal antibodies against modified nucleosides

For the establishment and testing of different validation methods, large quantities of antibodies are required. Therefore, we set out to generate our own monoclonal antibodies against specific base modifications, which were validated during the course of this study. We coupled individual nucleosides to a carrier protein and used the conjugate for immunization. The association to a carrier is necessary, as single nucleosides alone are too small to produce an efficient immune response. Ovalbumin (OVA) was used as an appropriate immunogenic carrier protein for immunization (Plescia and Braun 1967). To couple the modified nucleosides m^6A, m^5C, $m_2{}^6A$ and Ψ, a modified Erlanger-Beiser protocol was applied (Figure 1A, see Material and Methods for details). The first chemical reaction oxidizes and opens the ribose ring between the 2' and 3' position. An amino group of a lysine side chain, for example, can now efficiently react with the nucleoside leading to covalent coupling to the protein (Figure 1B). To validate and estimate coupling efficiencies, photometric analyses were performed (Figure 1C). OVA alone peaks at a wavelength of about 280 nm (Figure 1C, blue lines in all panels). Generally, the nucleoside-OVA conjugation shifts the OVA peak (purple lines) towards the free nucleosides (red lines). Coupling of m^6A (purple graph, panel I) and Ψ (purple graph, panel II) shifted the peaks towards the peak of m^6A or Ψ alone (Figure 1C, red graphs). For m^5C and $m_2{}^6A$

(panels III and IV) shifts were less pronounced since the individual components peak at a rather small window. Based on the peak intensities, coupling efficiencies were estimated to about 20% (data not shown). Similar results were obtained for coupling of the nucleosides to bovine serum albumin (BSA) as carrier protein (data not shown). OVA-conjugated nucleosides carrying m^5C, m^6A, $m_2{}^6A$ and Ψ, were used to immunize rats and mice (Figure 1D). Six to eight weeks after primary immunization, one boost injection was given and the immunized animals were sacrificed three days later. After fusion of splenic B cells and the myeloma cell line, all cells were evenly distributed in 96-well plates and hybridoma cells were selected. All outgrowing hybridoma cells were first screened in ELISA experiments for the expression of IgG antibodies specifically binding the respective modified nucleoside either as BSA-conjugates or as biotinylated oligonucleotides (Figure 1D, detection ELISA I/II). Capture ELISA experiments using BSA-conjugated nucleosides were performed to identify those supernatants containing IgG antibodies that are potentially useful for immunoprecipitation experiments (Figure 1D, capture ELISA). Unmodified oligonucleotides were included in all screenings as negative controls. Monoclonal hybridoma cell lines directed against m^6A, m^5C, $m_2{}^6A$ and Ψ were established and used for further validation studies.

Determination of dissociation constants (K_d)

In order to estimate the general performance of the antibodies in functional assays, we determined their affinities to free nucleosides (Figure 2). Equimolar mixtures of modified and unmodified nucleosides were incubated with the respective antibody. The mixture was subsequently centrifuged through a filter allowing molecules < 10kDa passing through. This procedure separates antibody-bound from -unbound

nucleosides, which can be used for K_d estimations (Figure 2A). Input samples and filtrates were further analyzed and quantified by HPLC. K_d values were calculated via scatchard plots (Figure 2B, Suppl. Figure 1) and a binding model was generated using data fitting (Figures 2C-F, Suppl. Figure 1; see Material and Methods for experimental details and K_d calculations). Using this method, we estimated the K_d of the α-m^6A clone 9B7 to 0.55 µM, clone 11D11 to 0.59 µM and clone 13G2 to 1.92 µM (Figure 2G). We next tested antibody clones against m^5C and identified affinities in a similar range with clone 32E2 showing the highest affinity of 0.39 µM (Figures 2D, G). Also, α-$m_2{}^6A$ clone 60G3 had a rather high affinity to the modified nucleoside (Figures 2E, G), while two clones directed against Ψ (26H5 and 27C5) showed only moderate affinities (Figures 2F, G). Our data therefore suggest that most of the tested antibodies have reasonably high affinity in solution (Figure 2G) at least to their nucleoside antigen and might be useful tools for further functional work.

'Dot blot' analysis

A common strategy to screen large numbers of hybridoma clones are western blots against antigens spotted onto nitrocellulose membranes – a method commonly referred to as 'dot blots'. BSA-conjugated nucleosides or oligonucleotides were immobilized and incubated with the respective antibodies. Methylene blue staining served as loading control (Figure 3A). Indeed, all tested clones (anti-m^6A 9B7; anti-m^5C 32E2; anti- Ψ 27C8 and anti-$m_2{}^6A$ 60G3) recognized their modified base epitopes while the unmodified base was not detected (Figure 3B). To evaluate whether antibodies recognize modified bases in a more natural environment, we modified the dot blot approach and spotted modified and unmodified oligonucleotides onto a nylon membrane and incubated it with the antibodies (Figure 3C). A widely

used commercially available antibody against m^6A (synaptic systems) was included for comparison. Although nylon membranes generated stronger antibody background, the tested hybridoma clones readily detected the modified but not the unmodified oligonucleotide with the exception of anti-Ψ 27C8, which did not work in this assay. This clearly underscores the need of different validation approaches to estimate antibody performance.

Determination of modified RNA enrichment

Although antibodies against RNA modifications are widely used in genome-wide profiling studies, it is often not known how specific they enrich modified RNAs compared to their unmodified counterparts adding uncertainty to many of these experiments. Therefore, we established two assays allowing for the determination of enrichment factors of modification-specific antibodies (Figure 4). In a first approach, we used chemically synthesized oligonucleotides containing either modified or unmodified bases (m^6A, m^5C, Ψ, m_2^6A). RNAs were ^{32}P-labeled, immunoprecipitated using the modification-specific antibodies and enrichments of modified compared to unmodified oligonucleotides were determined (Figures 4B-F). The α-m^6A clone 9B7 enriched m^6A-modified RNA by approximately 5-fold and is highly specific for m^6A (Figure 4B, left panel). The widely used commercially available m^6A-specific polyclonal antibody from synaptic systems showed moderate cross-reactivity with m^5C and m_2^6A in these experiments (Figure 4B, right panel). Furthermore, we tested whether the affinity of the antibodies differ when m^6A is within its natural RACH motif or when total RNA is added to simulate RIP experiments under realistic conditions (Suppl. Figure 3A). Indeed, under these conditions, both the m^6A-specific antibody 9B7 and the one from Synaptic Systems efficiently enriched modified RNA.

The α-m^5C clone 32E2 enriched highly specifically the m^5C-modified RNA significantly, other tested modifications were not recognized (Figure 4C). m^5C-specific antibodies from Diagenode or Cell Signaling only moderately enriched m^5C-containing RNAs, most likely due to the fact that they were raised against modified DNA (Figure 4D). A similar experiment was performed with the α-Ψ antibody 27C8 (Figure 4E). The antibody enriched Ψ-containing RNA by approximately 4-fold but seems to enrich m^5C even more. It is therefore not specific enough and the use of this antibody is clearly limited. Finally, we analyzed the m_2^6A-specific antibody clone 60G3 (Figure 4F). This antibody enriches m_2^6A-modified RNA 8-fold and does not cross-react with any other modification that we tested. Of note, even the structurally highly similar m^6A modification seems to be discriminated by this antibody.

In addition to the RIP experiments described above, we further developed a second approach to determine enrichment factors. In two in vitro transcription reactions, either the modified or the unmodified nucleotide was added (Slama et al. 2019). The modified RNA was transcribed in the presence of α-^{32}P-UTP and the unmodified was labeled with α-^{32}P-ATP. Both RNAs were mixed in different ratios and used for immunoprecipitation experiments using the modification-specific antibodies. After washing, the immunoprecipitated RNAs were fully hydrolyzed and the nucleotides were separated by thin layer chromatography (Figure 4G). Since α-^{32}P-UMP can be separated from α-^{32}P-AMP, the ratio between the two signals can be quantified and used for calculating the enrichment factor of the modified compared to the unmodified RNA. Using this approach, we tested α-m^6A 9B7, α-m^5C 32E2 and α-Ψ 27C8, because these modified nucleotides can be incorporated by T7 polymerase-mediated in vitro transcription. We tested two different conditions with 1% or 50% modified nucleotides being added to the in vitro transcription reaction. The α-m^6A

9B7 antibody enriched the modified RNA moderately by 1.5-fold (Figure 4H), which is similar to the enrichment factor of 1.5-2-fold by the commercial antibody from Synaptic Systems (Figure 4H, upper panel). When 50% modified RNA were used, up to 8-fold enrichment is achieved compared to unmodified RNA (Figure 4H, lower panel). We also tested two other α-m^6A antibody clones (11D11 and 13G2) and both displayed similar enrichment factors (Suppl. Figures 2A and B). We next tested α-m^5C 32E2 and determined a specific enrichment of more than 4-fold, when 1% of the RNA is modified (Figure 4I, upper panel). Two commercial antibodies (Diagenode, Cell signaling) show only mild enrichment. However, when 50% modified RNA is was applied, all three tested antibodies enriched modified RNA (Figure 4I, lower panel and Suppl. Figure 2C and D). Finally, we analyzed anti-Ψ clone 27C8 and did not find a specific enrichment of modified vs. unmodified RNA in both conditions (Figure 4J and Suppl. Figure 2E). This is consistent with the poor performance of the antibody in assays described before and demonstrates that our measurements are specific and reproducible in different approaches. In conclusion, our quantitative data allows for an estimation of antibody performance in solution reminiscent to conditions in genome-wide profiling experiments.

Binding to endogenous modified RNAs

Modification-specific antibodies are mainly used for RNA-profiling studies. Therefore, it is important to validate binding to endogenous RNAs carrying known modifications. To test this, we investigated whether the tested modification-specific antibodies generally bind to endogenous RNAs by crosslinking them to their RNA targets using UV light irradiation (Figure 5A). Such an UV crosslinking step is for example crucial in miCLIP experiments (Linder et al. 2015). The anti-m^6A antibody

clone 9B7, the commercial polyclonal antibody (Synaptic Systems), m^5C-specific clone 32E2, the m^5C-specific commercial monoclonal antibody clone 33D3 (Diagenode), the anti-Ψ antibody clone 27C8 and m_2^6A-specific clone 60G3 were incubated with total RNA isolated from HEK 293 cells and UV cross-linked. The RNA was partially digested, immunoprecipitates were radioactively labeled at the 5' end and transferred onto a nitrocellulose membrane (Figure 5B). Indeed, all antibodies tested except the m^5C-specific antibody clone 33D3 (Diagenode) were efficiently cross-linked and immunoprecipitated, while no signals were observed in non-cross-linked control reactions indicating that the antibodies bind and are efficiently crosslinked to endogenous RNA targets. However, crosslinking efficiencies differ between the antibodies possibly reflecting different modification levels or antibody affinities.

All four modifications, against which antibodies were established, are present in rRNA (Cecchini and Miassod 1979). Thus, we next asked whether these antibodies also specifically immunoprecipitate rRNA. Antibodies were coupled to beads and incubated with total RNA isolated from HeLa cells (Figure 5C). For specificity control, in vitro transcribed GFP mRNA was added to the mixture. After washing, the immunoprecipitated RNA was analyzed by northern blotting using probes against 18S and 5.8S rRNA, respectively. Antibodies α-m^6A 9B7, α-m^5C 32E2 and α-m_2^6A 60G3 efficiently immunoprecipitated 18S rRNA, while α-Ψ 27C8 enriched 5.8S rRNA albeit less efficient (Figure 5D, lanes 3 of each panel). IgG subtype-specific control antibodies confirmed the specificity of the analyzed antibodies (Figure 5D, lanes 2). These data highlight that endogenous target RNAs are bound by the tested antibodies and thus might be suitable for profiling experiments.

Since we found that the anti-m^6A antibodies 9B7 and 19B7 were efficiently crosslinked to endogenous RNAs by UV irradiation (Figure 5A, B), we performed miCLIP assays to determine m^6A modification of endogenous mRNA. We defined a gene set of 17158 peaks from MEF cells, which harbored at least one peak in each of the three replicates when performing miCLIP experiments with a commercial antibody (Abcam) (Supplementary Figure 3B). These genes represented 65.6%, 75.5% or 69.1% of the peaks in the three different replicates, indicating high reproducibility. We then analyzed whether our antibodies also pulled-down m^6A targets enriched by the Abcam antibody. Performing miCLIP with either 9B7 or 19B7 antibodies revealed a similar distribution of peaks over individual mRNAs like Cdk9 as the commercial antibody and displayed a typical enrichment of signals in the 3' UTR. In addition, C to T transition mutations occurred on the m^6A DRACH motif on mRNAs like Slc2a1 for all three antibodies tested (Supplementary Figure 3C and D). Moreover, about 5671 peaks were similarly identified by both of our newly generated anti-m^6A antibodies, and this overlap represented 32.7% or 25.9% of peaks with one m^6A peak in the samples generated with 9B7 or 19B7 antibodies (Supplementary Figure 3C). Collectively, these data indicate that the monoclonal antibodies can be used for CLIP experiments to determine the targets and positions of m^6A modifications.

Competition and elution experiments using modified and unmodified nucleosides

To further test for antibody specificity, competition experiments with the respective epitopes were performed. For α-m^6A 9B7, α-m^5C 32E2 and α-$m_2{}^6A$ 60G3, the modified nucleotide efficiently competed with 18S rRNA binding (Figure 5D, lanes 4). Competition with Ψ, however, inhibited binding of α-Ψ 27C8 to 5.8S rRNA rather

weakly (Figure 5D). The unmodified nucleotides did not show any competition with α-m^6A 9B7, α-m^5C 32E2 and α-Ψ 27C8. For α-m_2^6A 60G3, a mild reduction of 18S rRNA binding was observed when the unmodified nucleotide was added (Figure 5D). Thus, these data suggest that except of α-Ψ 27C8, antibodies α-m^6A 9B7, α-m^5C 32E2 and α-m_2^6A 60G3 bind their modified nucleotide targets specifically. Lower affinity and specificity of α-Ψ 27C8 is consistent with our previous results. To receive a more comprehensive picture of nucleotide competition and to assess optimal conditions for nucleoside-mediated elution, we performed titration experiments using nucleotide concentrations ranging from 10 nM to 100 µM and performed experiments as described above (Figure 5E). Consistently, 18S rRNA binding was strongly reduced when a concentration of 1 µM modified nucleotide was added to the washing buffer. As expected, unmodified nucleotides did not inhibit binding (Figure 5E). As observed in the experiments before, competition using α-Ψ 27C8 was less efficient and binding to the 18S rRNA was not completely lost even when 100 µM nucleotide concentrations are used (Figure 5E).

To increase specificity in immunoprecipitation experiments, bound factors can be eluted by an excess of the antigen. To test whether this strategy is applicable to modification specific antibodies as well, we immunoprecipitated the 18S rRNA from total RNA samples using α-m^6A 9B7 and α-m^5C 32E2 (Figure 5F and G). We incubated the immunoprecipitation reactions with 250 µM and 500 µM modified nucleosides and analyzed the eluates by Northern blotting. Indeed, an excess of both, m^6A and m^5C efficiently eluted the 18S rRNA from affinity beads, while the unmodified nucleosides had a much weaker or no effect (Figure 5G, lanes 5 and 9). Taken together, binding of α-m^6A 9B7 and α-m^5C 32E2 antibodies to 18S rRNA is

efficiently competed by the respective modified nucleosides and bound RNAs can be efficiently eluted.

Detection of modified nucleic acids by immunofluorescence

Antibodies are widely used for the visualization of intracellular localization patterns of their antigens. Therefore, we tested whether modification-specific antibodies are useful for immunofluorescence applications as well (Figure 6). In order to assess signal specificity for anti-m^{6}A antibodies, we knocked out METTL3, the enzyme that generates m^{6}A on mRNAs, from C643 cells and compared the signals and wild type (wt) cells. METTL3 knock out was confirmed by western blotting (Figure 6A). As expected, full digestion of poly(A)-selected RNAs from these cells and subsequent identification of m^{6}A nucleotides by HPLC analysis shows strong m^{6}A reduction in METTL3 knock out cells (Figure 6B and C). The remaining signal most likely originates from rRNA contaminations. Of note, a less abundant shorter band is detected on western blots, which could be a truncated METTL3 (Figure 6A). However, since m^{6}A levels are strongly reduced, we assume that such a putative truncated version is most likely non-functional. We next performed confocal microscopy-based immunofluorescence studies using the anti-m^{6}A clones as well as the commercial anti-m^{6}A antibody (Synaptic Systems) for comparison (Figure 6D, clone 19B7 is shown as example). Both antibodies strongly stained the cytoplasm of wt C643 cells while nuclear signals were not detected. METTL3 knock out C643 cells, however, show a markedly reduced cytoplasmic signal suggesting that both antibodies recognize m^{6}A-modified RNAs in immunofluorescence experiments. Non-coding RNAs such as rRNAs or snRNAs contain m^{6}A modifications but these modifications are independent of METTL3 function and thus the signal was only

reduced by approximately 40% as revealed by signal intensity measurements (Figure 6E). Using an alternative staining protocol optimized for staining chromatin-associated factors and modifications, the m^6A clone 19B7 showed a specific cytoplasmic staining, while other clones did not show specific signals (Suppl. Figure 4A-C).

M^5C is a very abundant modification on DNA and it is often found at promoter regions. It is enriched in distinct areas referred to as CpG islands and associated with epigenetic gene regulation processes (Jones 2012). We therefore tested whether α-m^5C antibodies also recognize modified DNA in immunofluorescence stainings (Figure 6F-H). Mouse-tail fibroblasts were permeabilized, treated with RNase A to test DNA specificity and stained with m^5C-specific antibodies (Figure 6F) (Ludwig et al. 2017). Both, the widely used commercial monoclonal antibody 33D3 (Active Motif) and our clone 32E2 detected distinct nuclear foci, which co-localized with DAPI-dense DNA structures (Figure 6F, middle and lower panels). These supra-chromosomal structures are termed chromocenters and correspond to clusters of constitutive pericentromeric heterochromatin that are composed by tandem repeats of m^5C enriched major satellite DNA (Casas-Delucchi et al. 2012). These data indicate that both clones recognize m^5C-modified DNA in immunostaining experiments. The clones α-m^5C 28F6 and 31B10, however, did not show specific signals suggesting that these antibodies are RNA-specific or not sensitive enough to allow the detection of modified DNA in immunofluorescence studies. We further tested different antibody dilutions and quantified the nuclear signal relative to the negative control (Figure 6G, dashed line, '2^{nd} only': secondary antibody only). The signal is lost when the antibody is linearly diluted suggesting an ideal dilution of 1:100 in such assays. Propidium iodide treatment, which stains not only DNA but also RNA showed a

moderate reduction of the nuclear signal when RNase A treatment was performed. The mild reduction shows that a small portion of the nuclear nucleic acid is indeed RNA (Suppl. Figure 4D). We next compared RNase A-treated with non-treated cells (Figure 6H). A dilution of 1:250 was chosen to avoid unspecific signals due to high antibody concentrations. Consistently with our previous results, RNase A treatment does not affect nuclear staining indicating that the two α-m^{5}C clones 33D3 (Active Motif) and 32E2 (this work) are DNA-specific under these experimental conditions. Since at least clone 32E2 detects efficiently modified RNA molecules, our results suggest that m^{5}C-modified RNAs are mainly found in the cytoplasm of these cells.

Taken together, modification-specific antibodies can be used for immunofluorescence as well, as exemplified by a number of antibodies that we tested.

M^{6}A detection in cell sorting experiments

In previous experiments, we have provided methods to validate antibody performance in solution und thus we asked whether we could also use such antibodies for Fluorescence-Activated Cell Sorting (FACS) experiments. As an example, we used m^{6}A-specific antibodies since knock out cell lines of the writer machinery are available and can be used for comparison (Figure 7). Flow cytometry analysis of wt mouse embryonic fibroblasts (MEFs) revealed that m^{6}A-modified RNA was robustly detected using anti-m^{6}A antibody clones 9B7, 11D11 and 19B7, as they also determined decreased m^{6}A abundance in Wtap-deficient MEF cells (Figure 7A, red overlay). Wtap is an essential component of the m^{6}A writer complex (43) and its expression was indeed lost in knockout cells as assessed by FACS with anti-Wtap antibodies (Figure 7B, red overlay). Of note, a commercially available antibody (Abcam) did not distinguish between wt and WTAP knock out cells. To rule out

clonal variation that may arise during drug-selection of MEF cell lines, we investigated whether these antibodies also specifically recognized m^6A-modified RNAs after acute depletion of Wtap. As shown in Figure 7C, the expression of Wtap was drastically reduced after retroviral transduction expressing the Cre recombinase, marked by co-expression of Thy1.1 in Wtapflox/flox MEF cells (Figure 7C). Consistently, all monoclonal antibodies recognized the difference of m^6A levels between Thy1.1+ (i.e. Cre-expressing, Wtap-deficient cells) and the Thy1.1– (WT cells) (Figure 7D, E). In summary, base modification-specific antibodies can in general be used for FACS experiments.

Discussion

Base-specific antibodies are widely used for the detection of modified RNAs and have been vital for the tremendous progress made in the analysis of m^6A functions. The success of m^6A-specific antibodies fostered the development of antibodies against other modifications. However, such modifications appear to be much less abundant on mRNAs and the used antibodies are often only partially validated. Therefore, not always reliable and sometimes even conflicting results were produced. These developments contributed to the view that antibody-based profiling of RNA modifications might be generally error-prone (Helm et al. 2019). Moreover, antibody-independent approaches have been developed for individual modifications and these methods produced also distinct results. For example, bisulfite-sequencing approaches were performed for m^5C modifications and led to very different results with mRNA targets ranging from very few to thousands (Squires et al. 2012; Edelheit et al. 2013; Hussain et al. 2013; Amort et al. 2017; Legrand et al. 2017; Huang et al. 2019). In addition, bulky chemical adducts are linked to specific modifications acting as

roadblocks in PCR reactions and thus defining the position of the modification. For example, CMC-addition to Ψ has been developed but highly varying datasets were reported (Zaringhalam and Papavasiliou 2016; Zhou et al. 2018). To validate these results, independent methods are required and therefore we set out to provide example strategies and methods for characterizing modification-specific antibodies We established monoclonal antibodies that specifically bind m^6A, m_2^6A, m^5C and Ψ modifications to obtain larger amounts of antibodies for testing since commercial antibodies are rather cost-intensive and could therefore not be included in all experiments.

A main shortcoming of available antibodies is that affinities and enrichment factors are often unknown. We therefore developed a method to define these key numbers. We found that all antibody clones, except antibodies against Ψ, bound free nucleosides in the low µM range (Figure 2G). However, it is important to note that these numbers might differ in the context of longer RNA molecules. Since the antibodies discriminate between modified and unmodified bases, it is likely that bases will also be efficiently bound when embedded into larger RNAs but affinities might differ. Another informative number for estimating antibody performance is the enrichment factor indicating 'fold enrichment' of modified over unmodified RNAs (Figure 4). In two different assays, we found that a commercially available antibody directed against m^6A (Synaptic Systems) as well as antibody clones developed in our laboratory enrich modified RNAs between 1.5 and 6-fold. Our m^5C-specific antibody enriched RNA 4-fold in a TLC-based assay (Figure 4I) and more than 100-fold in an independent RNA-IP-based approach with chemically synthesized RNA oligonucleotides (Figure 4D). Of note, commercial antibodies enriched m^5C-modified RNA only marginally. These and other antibodies were mainly generated to detected

m^5C in DNA. Thus, they may detect additional structural aspects of double stranded DNA, which are not present in short single-stranded RNA fragments. Nevertheless, the α-m^5C antibody clone 32E2 also recognized DNA in immunofluorescence staining experiments (Figure 6F) while the other established α- m^5C antibody clones did not stain DNA foci. In summary, for obtaining solid and reproducible results, it is important that affinities and efficiencies are considered when antibodies are combined with RNA-Seq approaches.

Immunofluorescence staining with m^6A antibodies detected m^6A RNAs in the cytoplasm and the signal was reduced in METTL3 knock out cells (Figure 6A-E). Since m^6A modifications on non-coding RNAs such as rRNAs or snRNAs are independent of METTL3, such a pattern is expected. However, it was unexpected that no nuclear signal was detected (Figure 6D) because the nuclear U6 snRNA, for example, carries one m^6A modification (Bohnsack and Sloan 2018). Furthermore, several YTH domain reader proteins are localized to the nucleus suggesting nuclear m^6A-modified RNAs are also present in this cellular compartment. Several scenarios explaining the lack of nuclear m^6A signals can be envisioned. First, the YTH domain covers the m^6A base and thus the epitope is not accessible for antibodies. Second, nuclear RNAs containing m^6A modifications are rather unstable and therefore of low abundance and not visible since m^6A might tag for rapid degradation. Third, the modified U6 snRNA could be deeply buried into the spliceosome and again the single modified base might not be accessible for antibodies. It is further conceivable that these aspects are also relevant for the cytoplasmic signal and the actual level of modified RNA in the cytoplasm might be even higher.

In summary, we generated and thoroughly validated a number of monoclonal antibodies. The antibody clones 9B7 (m^6A), 32E2 (m^5C) and 60G3 ($m_2{}^6A$) are

suitable for various applications such as RIP, immunofluorescence approaches, CLIP and FACS. However, we also emphasize that each individual base-specific antibody needs to be optimized regarding the experimental conditions and it is difficult to generalize such conditions in a single protocol. Concentration, dilution, salt conditions are very important and each antibody has to be optimized for the individual experimental settings. We strongly recommend that antibody conditions and performance in a number of different assays as exemplified here, should be assessed prior to usage and this should become a prerequisite rather than an option for publication.

Materials and Methods

Coupling of the nucleosides to ovalbumin

The coupling protocol of nucleosides to ovalbumin is based on the method described by (Erlanger and Beiser 1964). 25 mg of the nucleoside were dissolved in 1.25 ml 0.1 M $NaIO_4$ and incubated for 20 minutes at room temperature. 75 µl 1 M ethylene glycol were added and incubated for another 5 minutes at room temperature. 50 mg of ovalbumin were dissolved in 5 ml H_2O. The pH was adjusted to 9 using a 5 % K_2CO_3 solution. After adding the oxidized nucleoside to the ovalbumin solution, the mixture was stirred for 45 minutes, keeping the pH constantly at 9. A freshly prepared reduction solution (75 mg $NaBH_4$/5 ml H_2O) was then added to the conjugate and incubated over night at room temperature. Using 1 M formic acid, the pH was reduced to 5 – 6 and incubated for another hour at room temperature. After adjusting the pH to 8.5 using 1 M NH_3, the solution was gel filtrated on a Superose 12 column (GE Healthcare) in 0.2 M ammonium formate, pH 8.5. For analysis, the absorption of a defined amount of the conjugate was measured via UV spectroscopy. The molar

ratio of bound nucleoside per carrier protein was estimated by measuring the absorbance of the conjugate at 5 different wavelengths (250 nm, 260 nm, 270 nm, 280 nm and 290 nm) and fitting the measured data to the corresponding calculated absorption values. The spectrum of the conjugate was assumed to be the sum of nucleoside and carrier protein spectra. The absorbance was calculated by the extinction coefficients at the different wavelengths and the composition of the constituents. To obtain the "best fit"-composition of nucleoside and carrier protein, a grid search with a resolution of 0.1 µg was conducted using the sum-of-squares of the differences between measured and calculated absorption values as fit indicator.

Generation of monoclonal antibodies recognizing m^5C, m^6A and Pseudouridine (ψ) and ELISA screening

Approximately 50 µg of modified nucleobases coupled to ovalbumin (OVA) were dissolved in PBS, emulsified in an equal volume of incomplete Freund's adjuvant (Sigma) supplemented with 5 nmol CpG oligonucleotides (TIB Molbiol, Berlin), and injected both intraperitoneally (i.p.) and subcutaneously (s.c.) into Wistar rats and C57BL/6N mice. After 6 to 8 weeks, a boost with 50 µg of nucleobase-conjugated OVA without Freund's adjuvant was given 3 days before fusion. Fusion of the myeloma cell line P3X63-Ag8.653 with splenic B cells of immunized rat or mouse was performed according to standard procedures (Kohler and Milstein 1975). P3X63-Ag8.653 cells were cultured at 37 °C in a humidified 5 % CO_2 incubator in standard medium RPMI 1640 (Sigma/GIBCO), supplemented with 1% glutamine, 1 % non-essential amino acids, 1 % sodium pyruvate, 1 % penicillin/streptomycin (Sigma), and 2.5 % FCS (PAN). Hybridoma cells were cultured in standard RPMI 1640 medium supplemented with 20 % FCS and 2 % HT supplement (Life Technologies).

Hybridoma supernatants were positively tested in a solid-phase enzyme-linked immunoassay (ELISA) using the corresponding modified nucleobase coupled to BSA and negatively tested on non-modified nucleobase also coupled to BSA. To identify m^6A-specific hybridoma clones, 96-well polystyrene plates were coated with m^6A-conjugated BSA overnight at room temperature (m^6A-BSA: 2.5 µg/ml). In parallel, 96-well plates were coated with $m_2{}^6A$ and A (conc.: 2.5 µg/ml). To identify m^5C-specific antibodies, screening plates were coated with m^5C (positive screen) and C (negative screen), for screening plates were coated with Ψ (positive screen) or C and U (negative screens). After coating, plates were washed once with PBS, unbound sites were blocked with 2 % FCS in PBS for 20 min. After washing off unbound nucleobase BSA-conjugates, hybridoma supernatants (1:10 diluted) were added and incubated for 30 min. After another wash with PBS, plates were incubated for 30 min with a mix of HRP-coupled subclass-specific mouse anti-rat or rat anti-mouse secondary antibodies. After five washes with PBS, TMB substrate (1 Step Ultra TMB-ELISA; ThermoFisher Scientific Inc.) was added and the absorbance was measured at 650nm with a microplate reader (Tecan). To determine the specific antibody subclasses in a second validation after expansion of positive clones, respective BSA-nucleobase conjugates were coated onto 96-well polystyrene plates as described above, incubated with the hybridoma supernatants and then detected with HRP-coupled monoclonal mouse or rat antibodies specific for the different IgG subclasses of rat or mouse, respectively. Selected hybridoma cells of positively-tested supernatants specific for m^6A (13G2 rat IgG2a, 11D11 rat IgG1, 9B7 rat IgG1), m^5C (31B10 mouse IgG1/λ, 28F6 mouse IgG2b, 23E2 mouse IgG2c/λ), $m_2{}^6A$ (60G3 rat IgG2a) and Ψ (26H5 mouse igG2b, 27C8 mouse IgG2b) were cloned at least twice by limiting dilution.

Capture ELISA

Subclass-specific antibodies were coated onto microplates (200 mM Na_2CO_2 pH 9.5, 12 hours, at 4 °C). The following concentrations of subclass specific antibodies were used: mouse IgG1 and IgG2a: 3µg/ml; mouse Ig2b and rat IgG1: 5 µg/ml; rat IgG2a: 20 µg/ml. The plates were blocked with 2 % FCS in PBS. Hybridoma supernatants were incubated for 30 min at room temperature. After washing with PBS, the respective OVA-conjugated modified nucleotide was added at a concentration of 2.5 µg/ml and incubated for 30 min at room temperature. After incubation with a HRP-conjugated polyclonal ovalbumin-specific antibody and several PBS washes, TMB substrate was added and absorbance was detected with a microplate reader (Tecan).

Determination of the K_D of the antibodies

For the determination of the antibody bound fraction (BF) of a modified nucleoside, 6 samples of an equimolar mixture of the modified nucleoside with an internal standard (mostly the unmodified nucleoside) were prepared at 6 different concentrations. (Concentrations ranged from 75 µM to 250 µM). In order to maintain a constant ratio between the amount of the modified nucleoside and the internal standard, the dilutions were prepared out of a premixed stock solution with a concentration of 0.5 mM for each nucleoside. A volume of 20 µl of each of these mixtures were pipetted to 100 µl PBS (= Input sample) and to 100 µl PBS containing exactly the same amount of antibody for each sample (~ 150 µg) leading to initial nucleoside concentrations in the range of 12.5 µM to 41.7 µM. After incubation of the mixtures for 2 h at 4 °C4 °C, the unbound nucleosides of the antibody-containing samples were separated by centrifugation (2 min., 14,000 g) using a 10 kDa cut-off spin filter (Roti-Spin MINI,

Roth). A volume of 40 µl of each input and filtrate-sample was then applied to the HPLC with one replicate (see *HPLC analysis of nucleosides*). The two peaks of each chromatogram were integrated. The peak area of the modified nucleoside normalized to the peak area of the internal standard eventually gave the normalized peak areas of the modified nucleoside in the input sample (nucleoside input, NI) and in the filtrate of the antibody sample (nucleoside-antibody, NA) at the various concentrations. The antibody-bound fraction (BF) of the modified nucleoside can then be calculated by: BF = (NI – NA)/NI, which can be used to derive the concentrations of bound ([AbN]) and free nucleoside ([N]) from the initial Nucleoside concentration ($[N_0]$): [AbN] = BF x $[N_0]$ and [N] = (1 – BF) x $[N_0]$. To get a first estimation of the values for K_D and the maximal concentration of binding sites of the antibody ($[B_{max}]$), the ratio [AbN]/[N] was plotted against [AbN] to obtain a Scatchard plot (Scatchard 1949). From this, the K_D (dissociation constant) was estimated using the negative reciprocal value of the slope of the resulting regression line. The maximal concentration of binding sites is represented by the intersection point of the regression line with the x-axis. These estimates were then used to describe the binding with the following model:

$$[\mathrm{AbN}] = \frac{[\mathrm{Bmax}] * [\mathrm{N}]}{K_D + [\mathrm{N}]}$$

To enhance the accuracy of the model-parameters, the measured data points were fitted with nonlinear regression, whereby the residual sum-of-squares between model and measured data points was minimized using Excel solver. Finally, the 95%-confidence limits of the model parameters were determined via the model comparison-approach (F-test).

HPLC analysis of nucleosides

The nucleosides were resolved on a Hypercarb-column (5 µm, 100 x 2.1; Thermo Scientific) using the HPLC-system "WellChrom" from Knauer, equipped with Pump K-1001, Diode Array Detector K-2800, column oven and a Vacuum Degasser from Techlab GmbH (Germany). The experiments were done, detecting at wavelengths ranging from 260 to 280 nm. The resulting chromatograms were analyzed with the software ChromGate Client/Server Vers. 3.1.7. Depending on the particular nucleosides, three different gradients (purinfast2, pyrimidinfast2, pyrimidin50%ACN) of the buffers A (50 mM $NH_4CH_3CO_2$, pH 5.0), B (20% 50 mM $NH_4CH_3CO_2$, pH 5.0 / 80% acetonitrile) and C (50% acetonitrile) were applied at different temperatures (25°C, 55°C) and flow rates (0.2 ml/min, 0.25 ml/min). For details see the gradient tables in the supplemental information. For quantifying the percentage changes of the nucleoside concentrations between different samples, an equimolar amount of an internal standard (mostly the unmodified nucleoside) was added to the solution of the modified nucleoside. The peak area of the modified nucleoside was then normalized to the internal standard to correct for loading errors and/or unspecific binding during processing.

Dot blot

8 µg of RNA-oligo (Dharmacon, USA) were spotted on a nylon membrane. The RNA was EDC (1-ethyl-3-(3-dimethylaminopropyl) carbodiimide hydrochloride) cross-linked to the membrane. When using BSA-nucleotide conjugates, 20 µg was spotted and the membrane was baked at 80 °C for 1 h to crosslink. In both cases, the membrane was blocked in 1x TBS-T (150 mM NaCl, 10 mM Tris, pH 8.0, 0.1 % Tween) containing 5 % skimmed milk for 1 h at 4 °C. The first antibody (hybridoma) was diluted 1:5 in a 5 % skimmed milk solution in TBS-T and incubated over night at

4 °C, shaking. The secondary antibody (α-mouse and α-rat [Licor]) was diluted 1:10,000 in TBS-T containing 5 % skimmed milk and incubated for 1 hour. The documentation was conducted using the Odyssey scanner system (LI-COR Biosciences).

RNA-Immunoprecipitation

Total RNA from HEK293T cells was isolated using TRIzol® (Thermo Fisher Scientific). Several titration experiments have been conducted for the optimization of the RNA-immunoprecipitations. Thus, wide ranges of RNA, antibody and buffer concentrations and amounts are given in this protocol. Two different protocol setups for the RNA-immunoprecipitations were tested for these antibodies. For a part of the experiments, 0.1 - 100 µg of the respective purified antibody were coupled over night at 4 °C to 35 µl Protein G Sepharose beads (GE Healthcare). The coupled beads were washed thrice in RNA-IP buffer (150 - 750 mM LiCl, 0.5 % NP-40, 10 mM Tris-HCl, pH 7.5) or NET buffer (50 mM Tris, pH 7.5, 150 mM NaCl, 5 mM EDTA, 0.5 % NP-40, 10 % glycerol). Using 0.1 - 100 µg of the total RNA (~1 µg/µl) or 0.5 – 1 nmol of the RNA-oligos (ACGCGUm^6ACUUGA, ACGCGUAm^5CUUGA, AGCCUACCΨACUCAG, AGCCUACC$m_2{}^6$A CUCAG; Dharmacon, USA) the immunoprecipitation was conducted for 2 hours in 0.5 - 1 ml RNA-IP buffer. For the other setup, the antibody was incubated with the RNA in RNA-IP buffer for 2 hours. Protein G Sepharose beads were added and incubated for additional 2 hours. For the nucleotide-competition assay, 5 µM - 5 mM nucleotide (end concentration) was added and incubated for 1 additional hour. The setups were then washed once each with RNA-IP buffer, wash buffer I (RNA-IP buffer with 300 - 1000 mM LiCl) and wash buffer II (RNA-IP buffer with 450 - 1500 mM LiCl) or with NET buffer and twice

with NET wash buffer (NET buffer with additional 150 mM NaCl). For isolation of the RNA from the beads, either TRIzol® was used or the immune precipitated RNA was eluted from the beads by adding 250 – 500 µM nucleoside in 150 µl RIP buffer to the beads and incubating another 1 h at 4 °C, shaking. The RNA was precipitated using TRIzol® afterwards.

In vitro transcription with ^{32}P-labeled and modified NTPs, immune precipitation and digestion

DNA oligos with different lengths (880 bp, 100 bp and 50 bp) were *in vitro* transcribed in four different setups. For the first two transcriptions, modified NTPs of interest in different ratios of the total NTPs were used. In one of them, additional ^{32}P-UTP was added. The control setups were transcribed using unmodified NTPs and for the radioactive sample, ^{32}P-ATP was used. The four different samples were then DNase-digested and purified using the MEGAclear™ Transcription Clean-Up Kit (Ambion). For the cold samples, the concentration was determined using a NanoDrop Photometer, for the hot samples, the cpm-values were determined using the Cerenkov setting at a Scintillation-counter. The different RNA-solutions were then mixed to obtain equal cpm-values as well as same amounts (1.25 µg – 8 µg) for the modified and unmodified samples. These setups were then used for immune precipitation (for protocol: see RNA Immunoprecipitation). The precipitated RNA was digested using Nuclease P1 over night at 37 °C. The single nucleotides were afterwards analysed via 1D thin layer chromatography.

Thin layer chromatography (TLC)

The digestion with nuclease P1 and the TLC was conducted as described earlier (*e.g.*

(Grosjean et al. 2004). The digested RNA was spotted on a TLC-plate which ran in 66 % isobutyric acid and 1 % conc. ammonia for 3 – 4 hours. After drying, the signals were detected by exposure to a screen and scanning using a Phospho-imager (PMI, Bio-Rad).

Northern blot

Northern blot analysis was carried out as described earlier (Pall and Hamilton 2008). Briefly, the RNA was complemented with a 2 x RNA loading dye (formamide with bromophenol blue and xylene blue) and separated on 6 – 12 % Urea gels (Rotiphorese®, Roth) and semi-dry blotted onto a nylon membrane. The RNA was then either EDC cross-linked to the membrane and/or crosslinked via UV, depending on the size of the RNA of interest and hybridized overnight at 50 °C. ^{32}P-labeled 5'-GACGCTCAGACAGGCGTAGCCC-3' was used for 5.8 S rRNA and 5'-CATGCATGGCTTAATCTTTGAGACAAGC-3' for 18 S rRNA detection. To detect GFP mRNA, a probe with the following sequence was used: 5'-CCTTGAAGAAGATGGTGC-3'. The blot was then washed twice with wash buffer I (5 x SSC, 1 % SDS) and once with wash buffer II (1 x SSC, 1 % SDS). Signals were detected and documented using a Phospho-imager (PMI, Bio-Rad).

miCLIP analysis

The miCLIP experiments were executed largely following the protocol of (Grozhik et al. 2017). The fragmentation of the total RNA was performed with $ZnCl_2$ at 94 °C for 5 min as it is described in (Dominissini et al. 2013). The fragmented total RNA was incubated with the antibody of interest for 2 h, rotating and afterwards UV-crosslinked, using 254 nm and 150 mJ/cm^2. Using protein G dynabeads (Invitrogen),

the crosslinked RNA was precipitated for 2 h while rotating. After several washing steps, the RNA, attached to the antibody and beads was dephosphorylated and 5'-radiolabeled with γ-^{32}P-ATP. The beads were then resuspended in SDS-loading dye for elution. After SDS-PAGE, the gel was wet-blotted onto a nitrocellulose membrane at 90 V for 90 min. The radioactive signals were then detected using a Phospho-imager (PMI, Bio-Rad).

Western blot analysis

For performing western blot analysis, proteins were transferred onto a nitrocellulose membrane (GE Healthcare) using Towbin blotting buffer (192 mM glycine, 25 mM Tris/HCl pH 8.6, 20 % methanol). Membranes were blocked in 1 x TBST (150 mM NaCl, 10 mM Tris/HCl pH 8, 0.1 % Tween 20) containing 5 % skimmed milk for 1 h at 4 °C. After incubation with first and secondary antibody, the membrane was washed three times with 1 x TBST. α- αTubulin (mouse, Sigma, clone DM1A) and α-METTL3 (rabbit, Proteintech Europe) were used as primary and α-mouse and α-rabbit (Licor) were used as secondary antibodies. The documentation was conducted using the Odyssey scanner system (LI-COR Biosciences).

Immunofluorescence staining of human cells

C643 wildtype (WT) and METTL3 knockout cells (KO) cells were seeded on coverslips. The immunofluorescence experiments were conducted as described previously (Schraivogel et al. 2015). In short, fixation was performed, using 3.7 % PFA in PBS and stopped with 7.5 mg/ml glycine in PBS. Permeabilization was done with 0.2 % Triton-X 100 in PBS. After blocking in 1% BSA in PBS with 0.05 % Triton X-100, the first and secondary antibodies were incubated in blocking buffer.

After incubation with the antibodies, cells were mounted using Prolong Gold containing DAPI (Thermo Fisher Scientific–Life Technologies). Confocal microscopy was done on a TCSSP8 (Leica Microsystems) equipped with acousto-optical beam splitter, 405 nm laser (for DAPI) and argon laser (488 nm for α-rat and α-rabbit Alexa 488(Invitrogen)). Signal intensity was quantified using ImageJ (Wayne Rasband, NIH).

Immunostaining and Fluorescence of MTF cells

Mouse tail fibroblasts MTF-line3 (Guy et al. 2001) were seeded on gelatin coated glass coverslips one day prior immunostaining. To test the ability of the different antibody clones to detect genomic 5-methylcytosine, a previously described immunofluorescence staining protocol (Ludwig et al. 2017) was used. In brief, cells were fixed for 10 minutes with 3.7% formaldehyde, permeabilized for 20 min with 0.5% Triton X-100 and incubated with ice-cold methanol for 5 min. Afterwards, cells were incubated with or without 10 µg/mL RNaseA and blocked in 0.2% fish skin gelatin each for 30 minutes at 37 °C. Cells were incubated with the primary antibodies for 70 minutes at 37 °C. The primary antibody mix contained 2% BSA, 1x DNaseI Buffer (10 mM Tris-HCl, 2.5 mM $MgCl_2$, 0.5 mM $CaCl_2$), 25 U/mL DNaseI (Sigma Aldrich, St. Louis, MO, USA) and the respective mouse anti-m^5C clones, 28F6, 31B10 and 32E2 or the commercially available clone 33D3 (Active Motif, La Hulpe, Belgium). All clones were tested in dilutions of 1:100, 1:250 and 1:500 with an assumed concentration of 1 µg/µL. As control, samples were incubated with primary antibody mix without antibody (“2° only”). After incubation with the primary antibody, cells were washed three times with PBS-TE (0.01% Tween, 1 mM EDTA) and incubated with the secondary Alexa Fluor 488 conjugated goat anti-mouse-IgG

antibody (1:250, The Jackson Laboratory, Bar Harbor, USA) for 45 minutes at room-temperature. After washing with PBS-T (0.01% Tween), cells were counterstained with DAPI (1 µg/mL, Sigma Aldrich, St. Louis, MO, USA) and mounted in Moviol (Sigma Aldrich, St. Louis, MO, USA). To control for RNaseA activity, cells were treated as described for the immunostaining, with the difference that all antibodies in the mix were omitted and instead of DAPI, cells were stained with propidium iodide (1 µg/mL). The respective signals were quantified by imaging cells with the Operetta high-content screening system (PerkinElmer, UK), equipped with a Xenon fiber optic light source, a 20× long/0.45 NA objective, and 360-400, 460-490, and 520-550 nm excitation- as well as 410–480, 500–550 and 560-630 emission filters. Nuclei were identified by their DAPI or propidium iodide signal and in DAPI and m^5C stained nuclei the respective Alexa Fluor 488 signal was calculated. Intensities of stained nuclei were normalized by dividing all values by the mean nuclear Alexa Fluor 488 intensity of the "2° only" control. Normalized nuclear Alexa Fluor 488 values and mean nuclear propidium iodide values were plotted using R Studio. Also, statistical significance was tested with R Studio. Confocal Z stacks of immunostained cells were acquired with an Ultra-View VoX spinning disc microscope (PerkinElmer, UK) controlled by Volocity 6.3 (PerkinElmer, UK) and equipped with a 60x/1.45 NA Planapochromat oil immersion objective (voxel size, 0.12 x 0.12 x 0.5 µm; Nikon, Tokyo, Japan) and a cooled 14-bit CCD camera (cat.-no. C9100-50, Hamamatsu Photonics K.K., Hamamatsu City, Japan). Z-stacks were assembled into maximum Z-projections using ImageJ.

Cell culture of MEF cells

Mouse embryonic fibroblast (MEF) cells were cultured in Dulbecco's Modified Eagle's Medium (DMEM, GIBCO) supplemented with 10% (v/v) fetal bovine serum (FBS), 1,000 U/ml penicillin-streptomycin (GIBCO), and 10 mM HEPES, pH 7.4 (GIBCO) at 37 °C in 10% CO_2. To establish $WTAP^{-/-}$ MEF cells, retrovirus (mock or Cre) infection of MEFs was performed as described previously. Two days after virus infection, cells were diluted following trypsination and cultured in the presence of puromycin (1 μg/mL) for additional 3 days to select infected cell populations.

FACS sample preparation and analysis

After harvesting MEF WT and WTAP KO cells, they were washed with PBS. Cells were fixed with of 2 % Formaldehyde in PBS for 15 min at RT. Subsequently, the cells were permeabilized with 0.5 % saponin buffer in PBS. The first antibody was applied for 90 min at RT in 0.5 % Saponin buffer in PBS. Along the generated α-m^6A antibody clones, the α-m^6A antibody from Abcam (ab151230) was applied. After washing in PBS, the cells were incubated for 30 min at RT with the second antibody (Alex647-conjugated goat α-rat IgG, BioLegend, poly4054 or rabbit IgG, Invitrogen) in 0.5% Saponin buffer in PBS. For detection of the biotinylated antibodies, APC-conjugated streptavidin was applied. To stain WTAP, cells were fixed and permeabilized by using the Foxp3 / Transcription Factor staining buffer set (eBioscience) according to manufacturer's instructions. Anti-WTAP antibody (Proteintech, 60188) and FITC-conjugated goat antibody α-mouse IgG (BD Biosciences) were applied. After staining, cells were acquired on a FACS Canto II (BD Biosciences) device and samples were analyzed with FlowJo software.

Acknowledgements

We thank S. Ammon and C. Friederich for technical support. This work was supported by the Deutsche Forschungsgemeinschaft (DFG) grant SPP 1784/1 and 2 and the Bavarian Systems-Biology Network (BioSysNet) to GM and by DFG grant CA 198/10-1 to MCC.

References

Amort T, Rieder D, Wille A, Khokhlova-Cubberley D, Riml C, Trixl L, Jia XY, Micura R, Lusser A. 2017. Distinct 5-methylcytosine profiles in poly(A) RNA from mouse embryonic stem cells and brain. *Genome Biol* **18**: 1.

Batista PJ, Molinie B, Wang J, Qu K, Zhang J, Li L, Bouley DM, Lujan E, Haddad B, Daneshvar K et al. 2014. m(6)A RNA Modification Controls Cell Fate Transition in Mammalian Embryonic Stem Cells. *Cell Stem Cell* **15**: 707-719.

Bergquist PL, Matthews RE. 1962. Occurrence and distribution of methylated purines in the ribonucleic acids of subcellular fractions. *Biochem J* **85**: 305-313.

Bohnsack MT, Sloan KE. 2018. Modifications in small nuclear RNAs and their roles in spliceosome assembly and function. *Biol Chem* **399**: 1265-1276.

Bringmann P, Luhrmann R. 1987. Antibodies specific for N6-methyladenosine react with intact snRNPs U2 and U4/U6. *FEBS Lett* **213**: 309-315.

Carlile TM, Rojas-Duran MF, Zinshteyn B, Shin H, Bartoli KM, Gilbert WV. 2014. Pseudouridine profiling reveals regulated mRNA pseudouridylation in yeast and human cells. *Nature* **515**: 143-146.

Casas-Delucchi CS, van Bemmel JG, Haase S, Herce HD, Nowak D, Meilinger D, Stear JH, Leonhardt H, Cardoso MC. 2012. Histone hypoacetylation is required to maintain late replication timing of constitutive heterochromatin. *Nucleic Acids Res* **40**: 159-169.

Cecchini JP, Miassod R. 1979. Studies on the methylation of cytoplasmic ribosomal RNA from cultured higher plant cells. *Eur J Biochem* **98**: 203-214.

Coots RA, Liu XM, Mao Y, Dong L, Zhou J, Wan J, Zhang X, Qian SB. 2017. m(6)A Facilitates eIF4F-Independent mRNA Translation. *Mol Cell* **68**: 504-514 e507.

Dominissini D, Moshitch-Moshkovitz S, Salmon-Divon M, Amariglio N, Rechavi G. 2013. Transcriptome-wide mapping of N(6)-methyladenosine by m(6)A-seq

based on immunocapturing and massively parallel sequencing. *Nat Protoc* **8**: 176-189.

Dominissini D, Moshitch-Moshkovitz S, Schwartz S, Salmon-Divon M, Ungar L, Osenberg S, Cesarkas K, Jacob-Hirsch J, Amariglio N, Kupiec M et al. 2012. Topology of the human and mouse m6A RNA methylomes revealed by m6A-seq. *Nature* **485**: 201-206.

Edelheit S, Schwartz S, Mumbach MR, Wurtzel O, Sorek R. 2013. Transcriptome-wide mapping of 5-methylcytidine RNA modifications in bacteria, archaea, and yeast reveals m5C within archaeal mRNAs. *PLoS Genet* **9**: e1003602.

Erlanger BF, Beiser SM. 1964. Antibodies Specific for Ribonucleosides and Ribonucleotides and Their Reaction with DNA. *Proc Natl Acad Sci U S A* **52**: 68-74.

Feederle R, Schepers A. 2017. Antibodies specific for nucleic acid modifications. *RNA Biol* **14**: 1089-1098.

Fu Y, Dominissini D, Rechavi G, He C. 2014. Gene expression regulation mediated through reversible m(6)A RNA methylation. *Nat Rev Genet* **15**: 293-306.

Grosjean H, Keith G, Droogmans L. 2004. Detection and quantification of modified nucleotides in RNA using thin-layer chromatography. *Methods Mol Biol* **265**: 357-391.

Grozhik AV, Linder B, Olarerin-George AO, Jaffrey SR. 2017. Mapping m(6)A at Individual-Nucleotide Resolution Using Crosslinking and Immunoprecipitation (miCLIP). *Methods Mol Biol* **1562**: 55-78.

Grozhik AV, Olarerin-George AO, Sindelar M, Li X, Gross SS, Jaffrey SR. 2019. Antibody cross-reactivity accounts for widespread appearance of m(1)A in 5'UTRs. *Nat Commun* **10**: 5126.

Guy J, Hendrich B, Holmes M, Martin JE, Bird A. 2001. A mouse Mecp2-null mutation causes neurological symptoms that mimic Rett syndrome. *Nat Genet* **27**: 322-326.

Helm M, Lyko F, Motorin Y. 2019. Limited antibody specificity compromises epitranscriptomic analyses. *Nat Commun* **10**: 5669.

Helm M, Motorin Y. 2017. Detecting RNA modifications in the epitranscriptome: predict and validate. *Nat Rev Genet* **18**: 275-291.

Huang T, Chen W, Liu J, Gu N, Zhang R. 2019. Genome-wide identification of mRNA 5-methylcytosine in mammals. *Nat Struct Mol Biol* **26**: 380-388.

Hussain S, Sajini AA, Blanco S, Dietmann S, Lombard P, Sugimoto Y, Paramor M, Gleeson JG, Odom DT, Ule J et al. 2013. NSun2-mediated cytosine-5 methylation of vault noncoding RNA determines its processing into regulatory small RNAs. *Cell Rep* **4**: 255-261.

Jones PA. 2012. Functions of DNA methylation: islands, start sites, gene bodies and beyond. *Nat Rev Genet* **13**: 484-492.

Ke S, Alemu EA, Mertens C, Gantman EC, Fak JJ, Mele A, Haripal B, Zucker-Scharff I, Moore MJ, Park CY et al. 2015. A majority of m6A residues are in the last exons, allowing the potential for 3' UTR regulation. *Genes Dev* **29**: 2037-2053.

Ke S, Pandya-Jones A, Saito Y, Fak JJ, Vagbo CB, Geula S, Hanna JH, Black DL, Darnell JE, Jr., Darnell RB. 2017. m6A mRNA modifications are deposited in nascent pre-mRNA and are not required for splicing but do specify cytoplasmic turnover. *Genes Dev* **31**: 990-1006.

Kohler G, Milstein C. 1975. Continuous cultures of fused cells secreting antibody of predefined specificity. *Nature* **256**: 495-497.

Legrand C, Tuorto F, Hartmann M, Liebers R, Jacob D, Helm M, Lyko F. 2017. Statistically robust methylation calling for whole-transcriptome bisulfite sequencing reveals distinct methylation patterns for mouse RNAs. *Genome Res* **27**: 1589-1596.

Li X, Xiong X, Zhang M, Wang K, Chen Y, Zhou J, Mao Y, Lv J, Yi D, Chen XW et al. 2017. Base-Resolution Mapping Reveals Distinct m(1)A Methylome in Nuclear- and Mitochondrial-Encoded Transcripts. *Mol Cell* **68**: 993-1005 e1009.

Li X, Zhu P, Ma S, Song J, Bai J, Sun F, Yi C. 2015. Chemical pulldown reveals dynamic pseudouridylation of the mammalian transcriptome. *Nat Chem Biol* **11**: 592-597.

Linder B, Grozhik AV, Olarerin-George AO, Meydan C, Mason CE, Jaffrey SR. 2015. Single-nucleotide-resolution mapping of m6A and m6Am throughout the transcriptome. *Nat Methods* **12**: 767-772.

Littlefield JW, Dunn DB. 1958. Natural occurrence of thymine and three methylated adenine bases in several ribonucleic acids. *Nature* **181**: 254-255.

Liu J, Yue Y, Han D, Wang X, Fu Y, Zhang L, Jia G, Yu M, Lu Z, Deng X et al. 2014. A METTL3-METTL14 complex mediates mammalian nuclear RNA N6-adenosine methylation. *Nat Chem Biol* **10**: 93-95.

Lovejoy AF, Riordan DP, Brown PO. 2014. Transcriptome-wide mapping of pseudouridines: pseudouridine synthases modify specific mRNAs in S. cerevisiae. *PLoS One* **9**: e110799.

Ludwig AK, Zhang P, Hastert FD, Meyer S, Rausch C, Herce HD, Muller U, Lehmkuhl A, Hellmann I, Trummer C et al. 2017. Binding of MBD proteins to DNA blocks Tet1 function thereby modulating transcriptional noise. *Nucleic Acids Res* **45**: 2438-2457.

Maity A, Das B. 2016. N6-methyladenosine modification in mRNA: machinery, function and implications for health and diseases. *FEBS J* **283**: 1607-1630.

Matera AG, Terns RM, Terns MP. 2007. Non-coding RNAs: lessons from the small nuclear and small nucleolar RNAs. *Nat Rev Mol Cell Biol* **8**: 209-220.

Meyer KD, Jaffrey SR. 2017. Rethinking m6A Readers, Writers, and Erasers. *Annu Rev Cell Dev Biol*.

Meyer KD, Patil DP, Zhou J, Zinoviev A, Skabkin MA, Elemento O, Pestova TV, Qian SB, Jaffrey SR. 2015. 5' UTR m(6)A Promotes Cap-Independent Translation. *Cell* **163**: 999-1010.

Meyer KD, Saletore Y, Zumbo P, Elemento O, Mason CE, Jaffrey SR. 2012. Comprehensive analysis of mRNA methylation reveals enrichment in 3' UTRs and near stop codons. *Cell* **149**: 1635-1646.

Motorin Y, Helm M. 2011. RNA nucleotide methylation. *Wiley Interdiscip Rev RNA* **2**: 611-631.

Pall GS, Hamilton AJ. 2008. Improved northern blot method for enhanced detection of small RNA. *Nat Protoc* **3**: 1077-1084.

Plescia OJ, Braun W. 1967. Nucleic acids as antigens. *Adv Immunol* **6**: 231-252.

Polikanov YS, Melnikov SV, Soll D, Steitz TA. 2015. Structural insights into the role of rRNA modifications in protein synthesis and ribosome assembly. *Nat Struct Mol Biol* **22**: 342-344.

Safra M, Sas-Chen A, Nir R, Winkler R, Nachshon A, Bar-Yaacov D, Erlacher M, Rossmanith W, Stern-Ginossar N, Schwartz S. 2017. The m1A landscape on cytosolic and mitochondrial mRNA at single-base resolution. *Nature*.

Scatchard G. 1949. Equilibrium in non-electrolyte mixtures. *Chem Rev* **44**: 7-35.

Schraivogel D, Schindler SG, Danner J, Kremmer E, Pfaff J, Hannus S, Depping R, Meister G. 2015. Importin-beta facilitates nuclear import of human GW proteins and balances cytoplasmic gene silencing protein levels. *Nucleic Acids Res* **43**: 7447-7461.

Schwartz S, Bernstein DA, Mumbach MR, Jovanovic M, Herbst RH, Leon-Ricardo BX, Engreitz JM, Guttman M, Satija R, Lander ES et al. 2014. Transcriptome-wide mapping reveals widespread dynamic-regulated pseudouridylation of ncRNA and mRNA. *Cell* **159**: 148-162.

Slama K, Galliot A, Weichmann F, Hertler J, Feederle R, Meister G, Helm M. 2019. Determination of enrichment factors for modified RNA in MeRIP experiments. *Methods* **156**: 102-109.

Squires JE, Patel HR, Nousch M, Sibbritt T, Humphreys DT, Parker BJ, Suter CM, Preiss T. 2012. Widespread occurrence of 5-methylcytosine in human coding and non-coding RNA. *Nucleic Acids Res* **40**: 5023-5033.

Trixl L, Lusser A. 2019. The dynamic RNA modification 5-methylcytosine and its emerging role as an epitranscriptomic mark. *Wiley Interdiscip Rev RNA* **10**: e1510.

Yang Y, Fan X, Mao M, Song X, Wu P, Zhang Y, Jin Y, Yang Y, Chen LL, Wang Y et al. 2017. Extensive translation of circular RNAs driven by N6-methyladenosine. *Cell Res* **27**: 626-641.

Yue Y, Liu J, He C. 2015. RNA N6-methyladenosine methylation in post-transcriptional gene expression regulation. *Genes Dev* **29**: 1343-1355.

Zaringhalam M, Papavasiliou FN. 2016. Pseudouridylation meets next-generation sequencing. *Methods* **107**: 63-72.

Zhao BS, Roundtree IA, He C. 2017. Post-transcriptional gene regulation by mRNA modifications. *Nat Rev Mol Cell Biol* **18**: 31-42.

Zhou KI, Clark WC, Pan DW, Eckwahl MJ, Dai Q, Pan T. 2018. Pseudouridines have context-dependent mutation and stop rates in high-throughput sequencing. *RNA Biol* **15**: 892-900.

Zhou KI, Shi H, Lyu R, Wylder AC, Matuszek Z, Pan JN, He C, Parisien M, Pan T. 2019. Regulation of Co-transcriptional Pre-mRNA Splicing by m(6)A through the Low-Complexity Protein hnRNPG. *Mol Cell* **76**: 70-81 e79.

Figure legends

Figure 1. Synthesis of antigens for immunization: Coupling of nucleosides to ovalbumin. (A) Scheme for the conjugation reaction of the nucleosides to ovalbumin using the lysine NH_2-group as reactive group. After oxidative coupling, the nucleoside has no longer RNA specific properties, as the ribose ring is destroyed in the course of the reaction. (B) Schematic model of the coupling reaction of nucleoside (red) to ovalbumin (blue) to gain the conjugate (purple). (C) UV-spectra of the coupled conjugates (purple) vs. free ovalbumin (blue) and free nucleosides (red) are shown. The first spectrum shows m^6A-coupling followed by the spectra of m^5C, pseudouridine (Ψ) and of $m_2{}^6A$. (D) Outline of the generation of monoclonal antibodies against modified bases. Hybridoma cells were tested by detection and capture ELISAs using BSA-coupled nucleosides or biotinylated RNA-DNA-oligo hybrids.

Figure 2. Determination of K_D-values of antibodies against base-modifications. (A) Schematic outline of the experiment to determine K_D values of the antibodies. An equimolar mixture of modified and unmodified nucleotides was incubated with the respective antibodies tested and centrifugated through a filter with a cut-off allowing free nucleotides but not nucleoside-antibody complexes passing through. HPLC quantification of bound and unbound nucleosides were used for K_D estimation. (B) Example for a Scatchard Plot for antibody α- m^6A 9B7. (C) Binding model for antibody m^6A 9B7 shows the slow convergence towards saturation of the antibody binding capacity for the binding to m^6A nucleosides (grey squares). The black triangles depict the binding to $m_2{}^6A$ nucleosides. (D) Binding model of antibody m^5C 32E2, showing binding to m^5C nucleosides (squares) and to m^3C (triangles). (E) Estimation of the K_D-value for antibody $m_2{}^6A$ 60G3, using a binding model based on

m_2^6A (squares) or m^6A nucleoside binding (triangles). (F) The Binding model for α-Ψ antibody 27C8 was performed as described using Ψ nucleosides. For additional Scatchard plots and binding models for the antibody K_D-values, listed in Figure 2G, see Supplemental Figure 1. (G) Overview of the K_D-values of the different tested antibody clones against m^6A, m^5C, Ψ and m_2^6A. The last row indicates the respective nucleoside that was used for estimating the K_D-value.

Figure 3. Antibody specificity against base modifications using dot blot assays. (A) Scheme of the dot blot experimental setup. Unmodified/modified BSA conjugates or oligonucleotides (m^5C or C as examples) were spotted on a nylon membrane. After crosslinking and blocking, the membrane was incubated with the primary and secondary antibodies. Methylene blue stains nucleic acids and was used as a loading control. (B) Dot blot experiments, for which modified and unmodified BSA-nucleoside conjugate was used to assess the specificity of the antibodies α-m^6A 9B7, α-m^5C 32E2, α-Ψ 27C8 and α-m_2^6A 60G3. For m^6A, also the m_2^6A-BSA conjugate was spotted to investigate specificity between the two very similar modifications. (C) Dot blot experiments using a modified and a non-modified 12-mer RNA oligonucleotide as negative control. The antibody staining is shown on the left and the methylene blue staining as a loading control on the right. The dot blots for the antibodies α-m^6A 9B7 and Synaptic Systems, α-m^5C 32E2, α-Ψ 27C8 and α-m_2^6A 60G3 are depicted.

Figure 4. Qualitative Enrichment of modified vs. non-modified RNAs using quantitative immunoprecipitation and a thin-layer chromatography-based assay. (A) Schematic overview of the experimental setup. Modified (m^5C as example) and

unmodified or differently modified (depicted as X) chemically synthesized oligonucleotides of 12 nts in length were radioactively 5'labeled. Oligonucleotides were subjected to immunoprecipitation using the indicated antibodies. After washing, the radioactive signals (cpm-values) of the immunoprecipitated RNAs as well as the input samples were measured using a scintillation detector (Cerenkov measurement) and enrichment factors were calculated. (B - F) Depiction of the enrichment of the antibodies α-m^6A 9B7, polyclonal α-m^6A (Synaptic Systems), α-m^5C 32E2, α-m^5C (Diagenode), α-m^5C (Cell Signaling), α-Ψ 27C8 and α-$m_2{}^6A$ 60G3 by using the RNA-IP-based approach, shown in A. (B) shows the results for the m^6A antibodies 9B7 and polyclonal Synaptic Systems, (C) the enrichment with antibody α-m^5C 32E2, (D) enrichment of α-m^5C from Diagenode or Cell Signaling, (E) of antibody clone Ψ 27C8, and (F) depicts the enrichment of the antibody α-$m_2{}^6A$ 60G3. Experiments were conducted in triplicates. (G) Workflow for enrichment factor using *in vitro* transcription (ivt), antibody enrichment and thin layer chromatography (TLC). Ivt with modified (m^5CTP as example) and radiolabeled NTPs and immunoprecipitation, the RNA was hydrolyzed with the nuclease P1 and analyzed by TLC. (H) Evaluation of m^6A IP-TLC experiments as described above using 1 % (upper panel) or 50 % (lower panel) m^6ATP for the ivt and analysis of the monoclonal m^6A antibody clone 9B7 and the polyclonal m^6A-antibody from Synaptic Systems. The light grey bars show the normalized signal intensities, corresponding to the precipitated unmodified RNA, the dark grey bars show the same for the precipitated modified RNAs. Experiments were conducted in triplicates. (I) Evaluation of m^5C IP-TLC experiments using 1 % (upper panel) and 50 % (lower panel) m^5CTP for the *ivt* and analysis of m^5C antibody clone 32E2 and commercially available m^5C-specific antibodies from Diagenode and Cell Signaling. Experiments were conducted in triplicates. (J)

Determination of the enrichment factors of antibody α-Ψ 27C8 based on the RNA-IP and TLC experiments. For these experiments, 1 % (upper panel) and 50 % (lower panel) ΨTP was used for the ivt. TLCs and further evaluations of other antibodies that we tested can be found in Supplemental Figure 2.

Figure 5. Immunoprecipitation of endogenous modified RNAs. (A) Overview of the workflow for crosslinking modification-specific antibodies to endogenous RNAs. Fragmented total RNA from HEK293T cells was cross-linked to the antibody of interest using 254 nm UV light. RNA was immunoprecipitated, radiolabeled and the RNA-antibody complexes were analyzed by SDS-PAGE. As a negative control, a non-irradiated setup was used. (B) Autoradiographs of the crosslinking experiments described in (A) using m^6A antibody clones 9B7, Synaptic Systems (I), m^5C antibody clone 32E2 and the commercial antibody 33D3 (Diagenode) (II), α-Ψ antibody clone 27C8 (III) and m_2^6A antibody clone 60G3 (IV). (C) Binding competition assays between endogenous RNAs and free nucleosides. Specific antibodies were used for immunoprecipitation from 2 µg total HEK293T cell RNA and 75 ng GFP mRNA as a negative control spike-in. To test for specificity, 100 µM of the respective modified (e.g. m^5C) and unmodified nucleoside (e.g. C) were added to the immunoprecipitation as competitor. The immunoprecipitated RNA was separated on an RNA gel and blotted onto a nylon membrane. A probe against the 18S or 5.8S rRNA and a probe against the GFP mRNA were used for detection. (D) Northern blots for endogenous 18S and 5.8S rRNAs as well as GFP mRNA spike-ins. The antibodies α-m^6A 9B7, α-m^5C 32E2, α-Ψ 27C8 and α-m_2^6A 60G3 were used. Input samples (200 ng total RNA and 75 ng GFP mRNA) are shown in lanes 1 and immunoprecipitates using an IgG control antibody used as a negative control in lanes 2. The upper panels show the

signals of the 18S/5.8S rRNA, the lower ones for the spiked-in a GFP mRNA. Lanes 3 show signals for untreated IP experiments, lanes 4 depict the signals of an IP competed with modified and lanes 5 with unmodified nucleosides. (E) Competition titration experiment of antibodies α-m^6A 9B7, α-m^5C 32E2 and α-Ψ 27C8. Different concentrations ranging from 10 nM to 100 µM of modified and unmodified nucleosides were added to RNA-IP experiments. For detection, probes against 18S and 5.8S rRNA were used. (F) Nucleoside-mediated elution of antibody-bound endogenous 18S rRNA. (G) Northern blots of immunoprecipitation experiments using antibodies α-m^6A 9B7 and α-m^5C 32E2. RNA either extracted from beads (lanes 2-5) or from specifically eluted supernatants (lanes 6-9) were analyzed by Northern blotting. Lane 1 shows the input of the immunoprecipitation experiments.

Figure 6. Immunofluorescence stainings of C643 wild type (WT) and METTL3 knockout (KO) cell lines using α-m^6A antibodies and immunofluorescences of MTF cells stained with α-m^5C clone 32E2 detecting genomic m^5C. (A) Western blot analysis of C643 WT and METTL3 KO cell lysates, probed with antibodies against METTL3 and α-Tubulin as a loading control. (B) Verification of m^6A levels in the mRNA of C643 cells of WT compared to METTL3 KO by HPLC measurements. (C) Integrated values from (B) were normalized to WT and are given in percentage. (D) Immunofluorescences of WT and METTL3 KO cells. The cells were stained with α-m^6A 19B7 (upper part) and polyclonal α-m^6A Synaptic Systems (lower part). The DAPI staining (blue) shows the nuclei of the cells, in green, the m^6A signals are shown. The right panel displays merged stainings. (E) Quantification of the signal intensities of the immunofluorescence staining of WT and METTL3 KO cells shown in A. For quantification, 30 cells each were analyzed. (F) Exemplary pseudo-colored

maximum confocal Z-projections of RNaseA treated mouse tail fibroblasts (MTFs), stained with the indicated m^5C antibodies diluted 1:250. An Alexa Fluor 488 conjugated secondary antibody was used to visualize the primary antibodies. DNA was stained with DAPI (scalebar, 10 µm). (G) Boxplots showing the normalized mean nuclear Alexa Fluor 488 intensities. Nuclear levels were normalized against cells stained without any primary antibody ("2^{nd} only"). The outcome of three tested antibody dilutions, 1:100, 1:250, 1:500, is shown (n > 15000). The dashed line indicates the median of "2^{nd} only" cells. (H) Boxplots showing the normalized mean nuclear levels of Alexa Fluor 488 in MTF cells treated with or without RNaseA and stained with an antibody dilution of 1:250 (n > 40000). Signal levels of Alexa Fluor 488 were normalized against control cells that were only stained with the secondary antibody. The dashed line indicates the median of cells, stained without primary antibody.

Figure 7. (A) Flow cytometry comparison of MEF cells stained with purified anti-m^6A specific rat monoclonal antibodies or polyclonal commercial anti-m^6A antibodies (Abcam). Staining with a secondary anti-rat antibody served as a negative control. Data are representative of three independent experiments. (B, C) Deletion of Wtap in Wtap-/- MEF cells after puromycin selection (B) or acute deletion via Cre transduction of MEF cells at Day 4 (C) was confirmed via anti-Wtap staining. (D-E) Flow cytometry analysis of m^6A and Thy1.1 (Cre) in Cre-transduced MEF cells Day 7 is shown as contour plot (D, upper panel) indicating the gates used to overlay m^6A levels that are present in the Thy1.1 positive (D, lower panel, red) and Thy1.1 negative (D, lower panel black) cells. (E) The fold change of the geometric mean

fluorescence intensity (gMFI) of Wtap (C) or m^6A (D, lower panel) is shown displayed.

Supplemental Figure 1. Additional Scatchard plots and binding models for the different antibodies, determining the K_D-value. The figure shows Scatchard plots and binding models of the antibodies to determine the K_D-values, which are shown in figure 2H. (A-C) Scatchard Plots (upper graphs) and binding models (lower graphs) of the m^6A antibodies 9B7, 13G2 and 11D11. (D-F) The same is shown for the m^5C antibodies 32E2, 31B10 and 28F6. (G and H) K_D determination of α-Ψ antibody clones 26H5 and 27C8. (I) Scatchard plot and binding model for the $m_2{}^6A$ antibody 60G3.

Supplemental Figure 2. Estimation of the enrichment via Thin-Layer Chromatography (TLC). (A) Thin layer chromatography (left panel) and the graphical evaluation (right panel) of m^6A IPs and comparison of self-established m^6A antibodies (α-m^6A 11D11, α-m^6A 13G2 and α-m^6A 9B7) vs. a polyclonal m^6A-antibody from Synaptic Systems. The commercial antibody and clone 9B7 are shown in Figure 4. (B) TLC and evaluation of TLCs using 1 % m^6ATP for the *in vitro* transcription (ivt). Experiments were conducted in triplicates. (C) Determination of the enrichment factors of the different antibodies against m^5C using 1 % m^5CTP for ivt and comparison with the commercial monoclonal antibody (33D3, Diagenode). Evaluation based on triplicates of RNA-IP and TLC experiments. (D) TLC of a titration assay using m^5C antibody 32E2. The ratio of m^5C to unmodified C in the *in vitro* transcription was varied between 10 and 50 %. The RNA was titrated from 2.5 to 16 µg total input for each setup. Below, the evaluation and graphical depiction of

the TLCs are shown. (E) Analyses of RNA-IP and TLC experiments conducted with different antibodies against Ψ and determination of the enrichment factors. In the left part, 1 % ΨTP, in the right part, 50 % ΨTP was used for ivt.

Supplemental Figure 3. RIP and CLIP experiments using m^6A-specific antibodies. **(A)** RNA oligonucleotides were incubated with the indicated antibodies and enrichment was calculated as shown in Figure 4B-F. Total RNA from HEK 293 cells was added to simulate a natural RNA environment. (B-D) Comparing m^6A-specific antibodies in miCLIP experiments. Venn diagram showing the overlap of peaks identified by miCLIP using the commercial (Abcam) antibody (B) and biotinylated-9B7 or 19B7 monoclonal antibodies. (D) An alignment of corresponding m^6A peaks from different antibodies over the Cdk9 transcript is shown in B. Red dots indicate mutation sites on the transcript. C-to-T transition on the motif is shown in red letters.

Supplemental Figure 4. Immunofluorescences of MTF cells stained with α-m^6A antibodies detecting genomic m^6A. (A) Exemplary immunofluorescence images of RNaseA treated and non-treated mouse tail fibroblasts (MTFs), stained with the α-m^6A antibody 19B7 diluted 1:250. An Alexa Fluor 488 conjugated secondary antibody was used to visualize the primary antibody. DNA was stained with DAPI (scalebar, 10 µm). (B) Boxplots showing the normalized mean nuclear Alexa Fluor 488 intensities in MTF cells treated with or without RNaseA. Nuclear levels were normalized against cells stained without any primary antibody ("2° only"). The outcome for the three tested antibody dilutions, 1:100, 1:250, 1:500, is shown ($n > 15000$). The dashed line indicates the median of "2^{nd} only" cells. (C) Boxplot showing the mean nuclear levels of propidium iodide in cells treated with or without RNaseA

(n > 60000). Significance was tested with student's t-test. (D) Boxplot showing the mean nuclear levels of propidium iodide in cells treated with or without RNaseA (n > 60000) of the cells, shown in Figure 6F.

Table 1: Summary of antibody validation results

Modification	Antibody clone	apparent K_D-value	RNA-IP	TLC	IF	Crosslink	FACS
m^6A	13G2	+	n.a.	++	n.a.	n.a.	n.a.
	11D11	+++	++	++	-	+	++
	9B7	+++	++	++	++	+++	+++
	19B7	n.a.	+	n.a.	+++	+++	+++
m^5C	31B10	++	n.a.	-	-	n.a.	n.a.
	28F6	++	n.a.	+	-	n.a.	n.a.
	32E2	+++	+++	+++	+++	+++	n.a.
Ψ	26H5	-	n.a.	n.a.	n.a.	n.a.	n.a.
	27C8	-	-	+	n.a.	++	n.a.
m_2^6A	60G3	++	++	n.a.	n.a.	+	n.a.

K_D: dissociation constant, IP: immunoprecipitation, TLC: thin layer chromatography-experiment, IF: immunofluorescence, FACS: fluorescence-activated cell sorting; +: medium performance in the experiment, ++: good performance in the experiment, +++: very good performance in the experiment, n.a.: not analyzed.

A

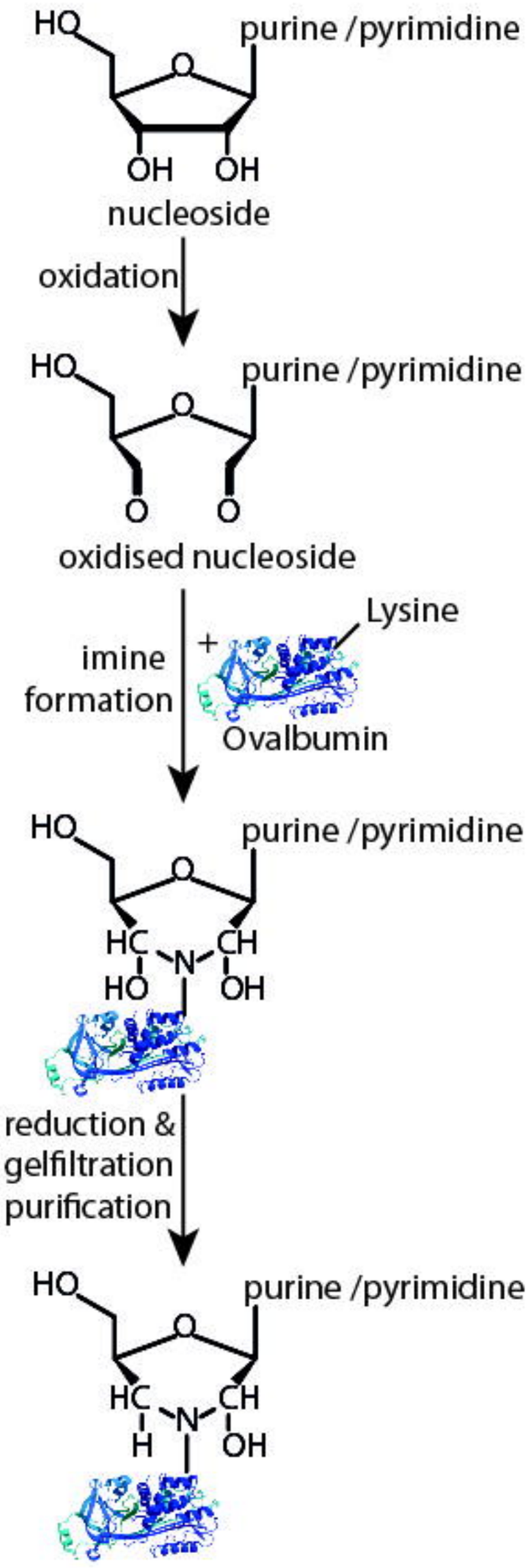
HO
purine /pyrimidine
OH OH
nucleoside
oxidation
HO
purine /pyrimidine
O O
oxidised nucleoside
imine formation
+
Lysine
Ovalbumin
HO
purine /pyrimidine
HC N CH
HO OH
reduction & gelfiltration purification
HO
purine /pyrimidine
HC N CH
H OH

B

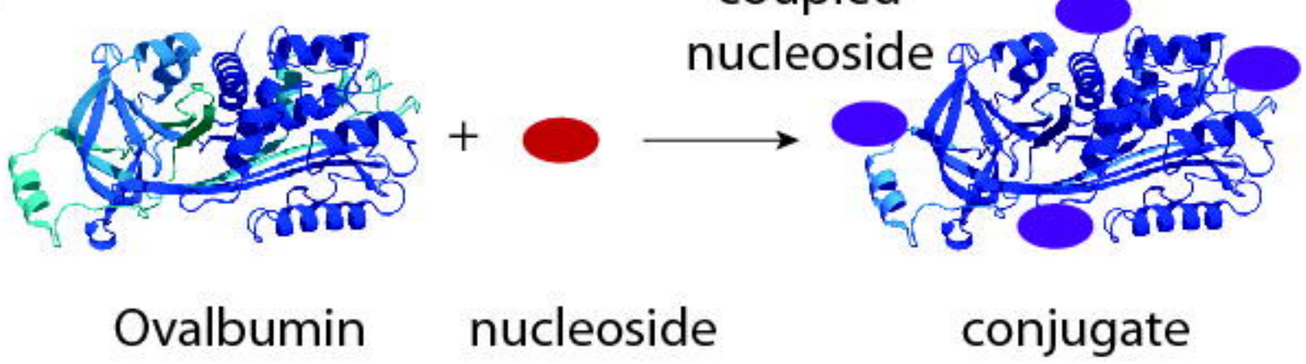
coupled nucleoside
+
Ovalbumin
nucleoside
conjugate

C

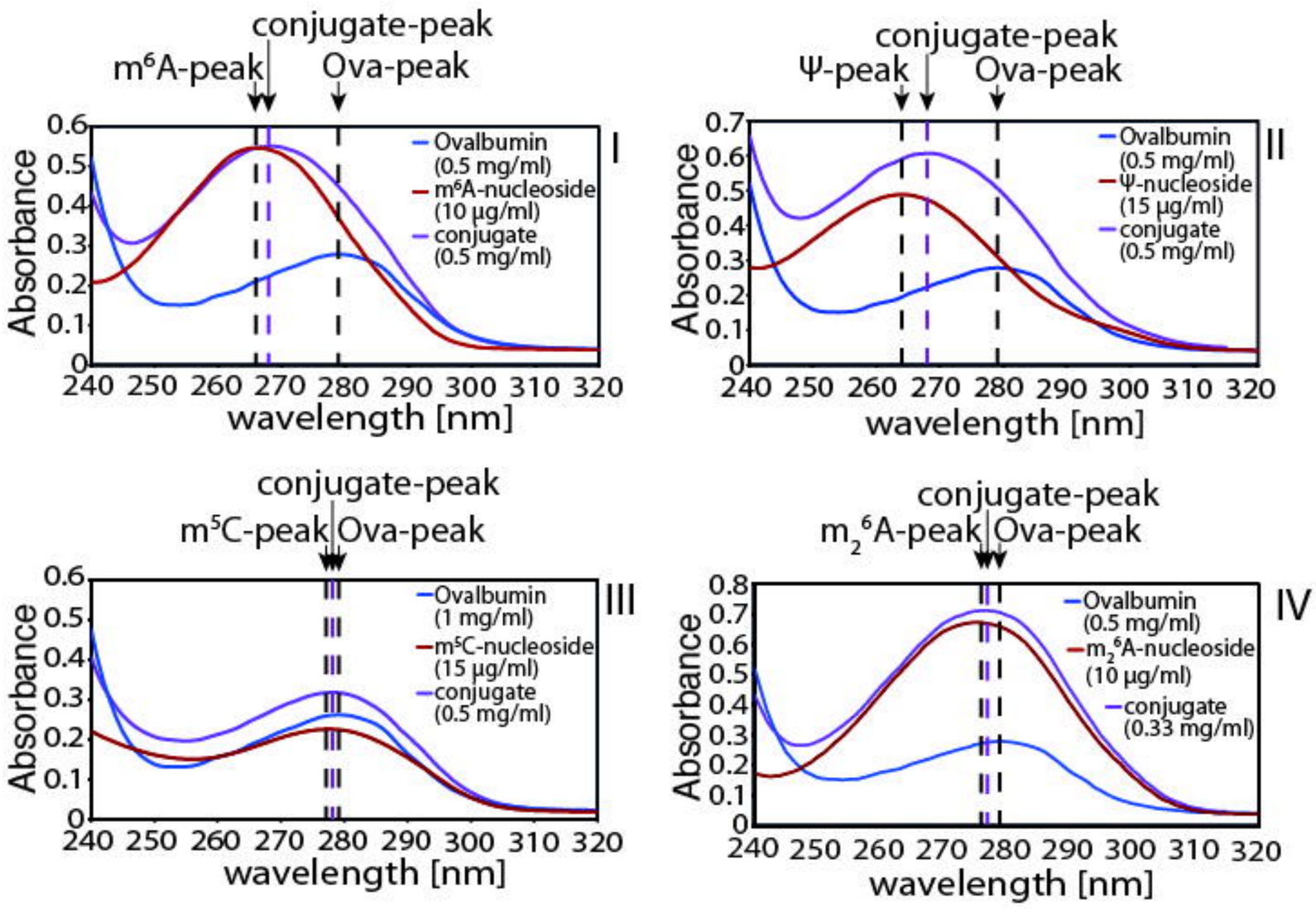
conjugate-peak
m⁶A-peak
Ova-peak
Absorbance
wavelength [nm]
Ovalbumin (0.5 mg/ml)
m⁶A-nucleoside (10 µg/ml)
conjugate (0.5 mg/ml)
I
Ψ-peak
Ψ-nucleoside (15 µg/ml)
II
m⁵C-peak
m⁵C-nucleoside (15 µg/ml)
Ovalbumin (1 mg/ml)
III
m₂⁶A-peak
m₂⁶A-nucleoside (10 µg/ml)
conjugate (0.33 mg/ml)
IV

D

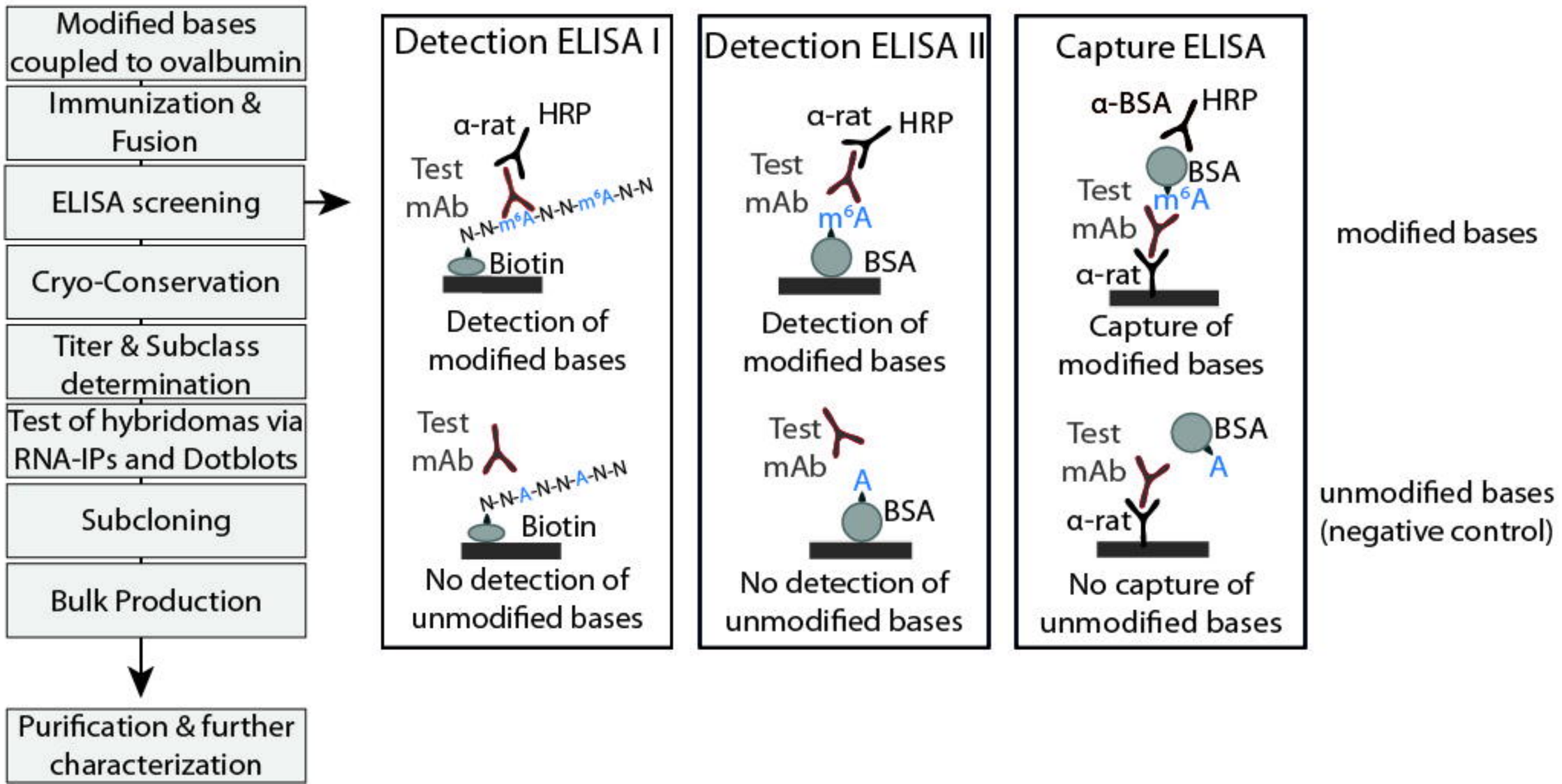
Modified bases coupled to ovalbumin
Immunization & Fusion
ELISA screening
Cryo-Conservation
Titer & Subclass determination
Test of hybridomas via RNA-IPs and Dotblots
Subcloning
Bulk Production
Purification & further characterization
Detection ELISA I
α-rat
HRP
Test mAb
N-N-m⁶A-N-N-m⁶A-N-N
Biotin
Detection of modified bases
N-N-A-N-N-A-N-N
No detection of unmodified bases
Detection ELISA II
m⁶A
BSA
A
Capture ELISA
α-BSA
Capture of modified bases
No capture of unmodified bases
modified bases
unmodified bases (negative control)

A

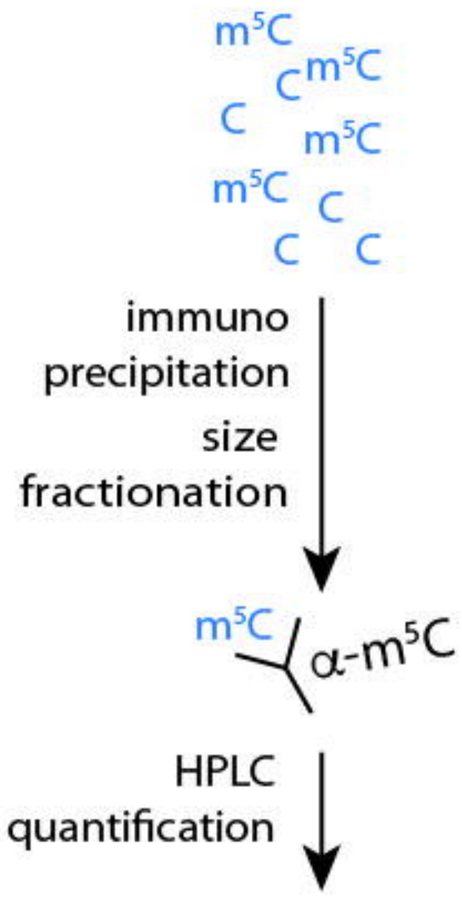

B

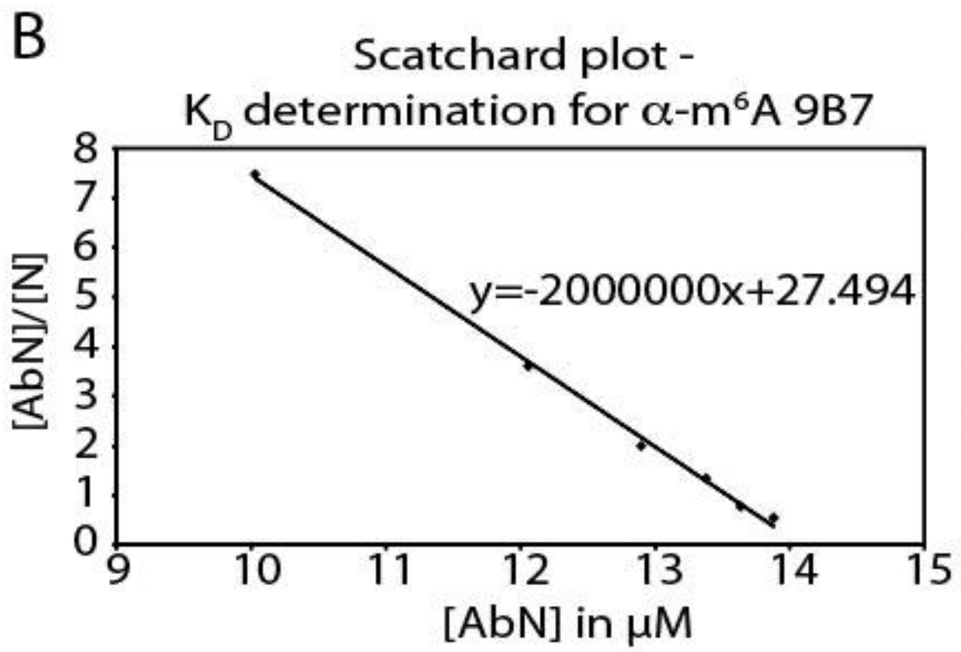

C

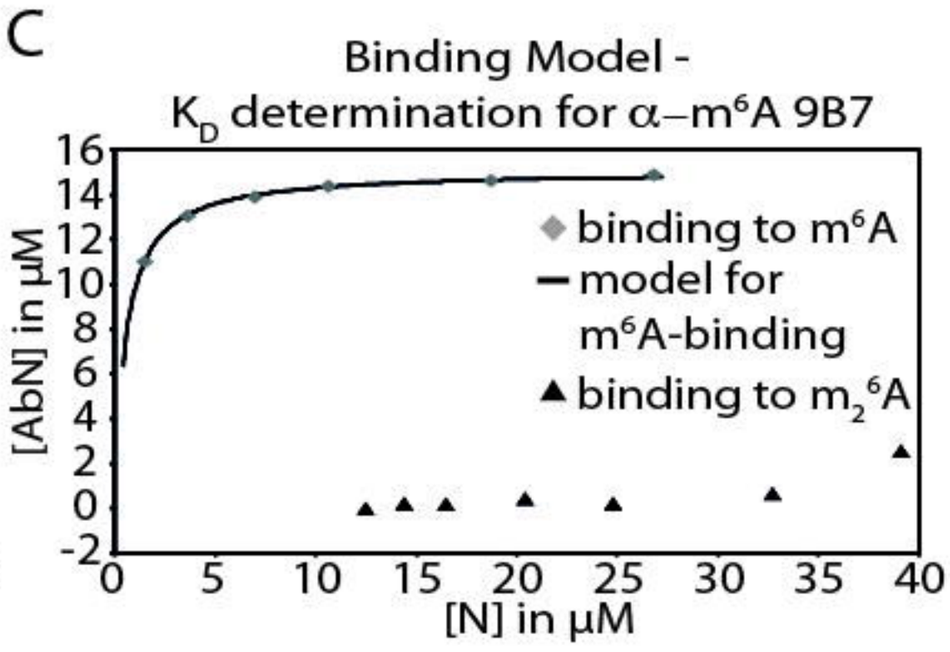

D

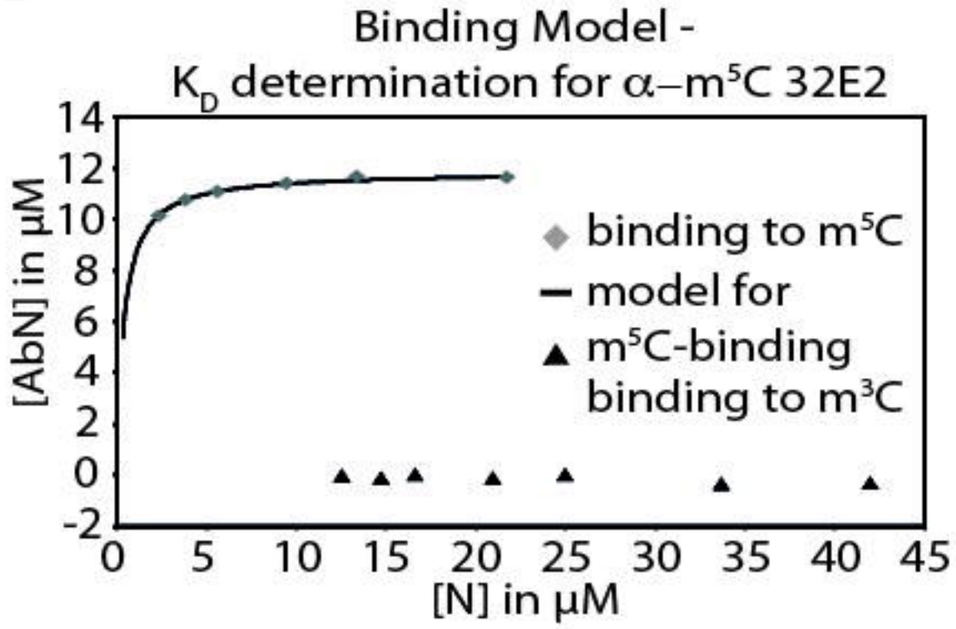

E

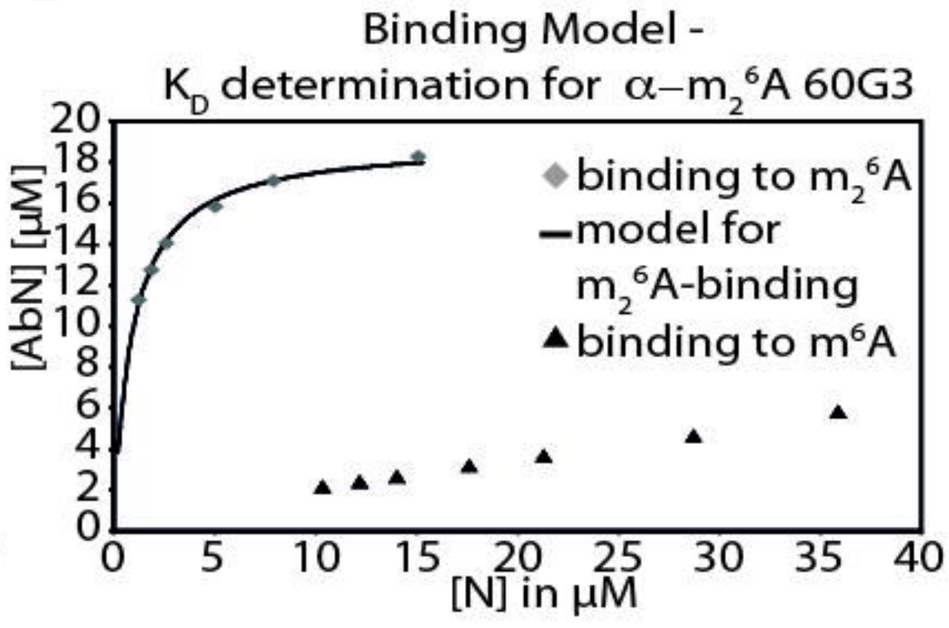

F

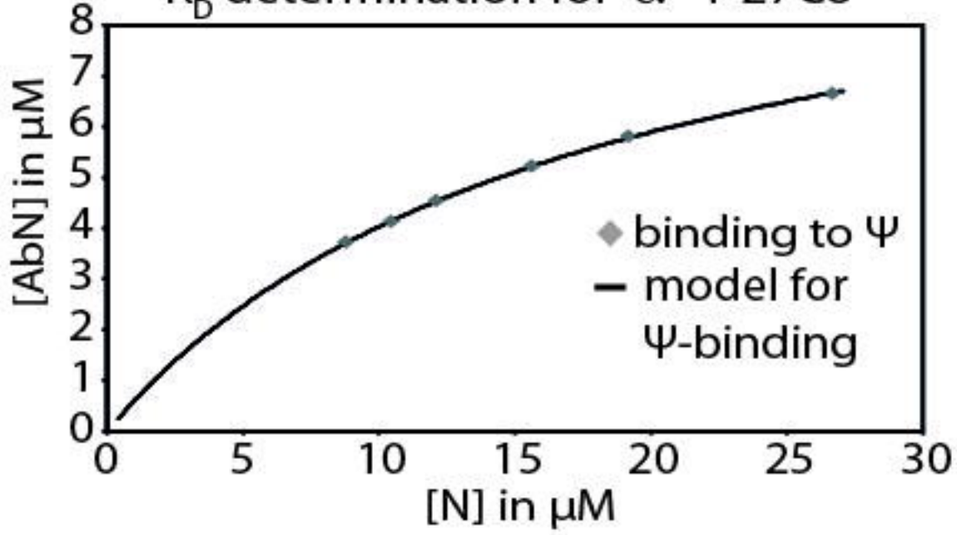

G

Modification	Antibody clone	apparent K_D-value (nucleoside) [µM]	control nucleoside
m^6A	13G2	1.92	A
	11D11	0.59	A
	9B7	0.55	A
		0.89	m_2^6A
		0.60	m^1A
m^5C	31B10	1.14	C
	28F6	1.5	C
	32E2	0.39	C
		0.68	m^3C
Ψ	26H5	38.12	U
	27C8	17.18	U
m_2^6A	60G3	0.89	A
		1.15	m^6A

A

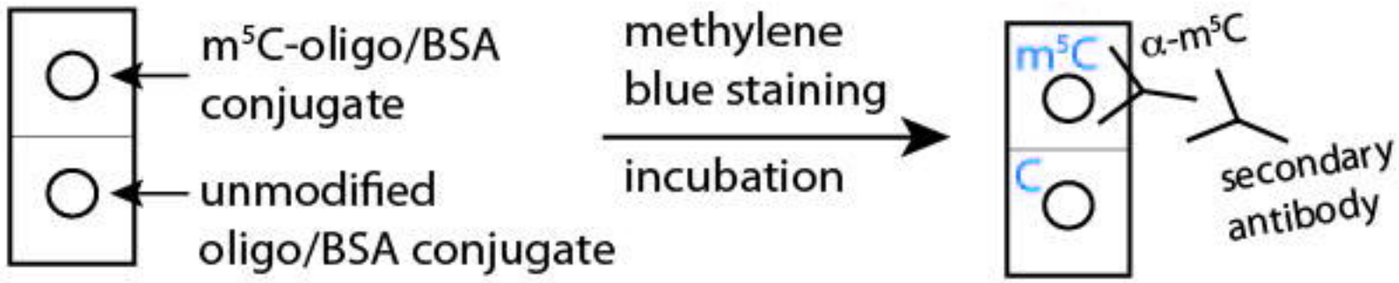
m5C-oligo/BSA conjugate
unmodified oligo/BSA conjugate
methylene blue staining
incubation
m5C
C
α-m5C
secondary antibody

B

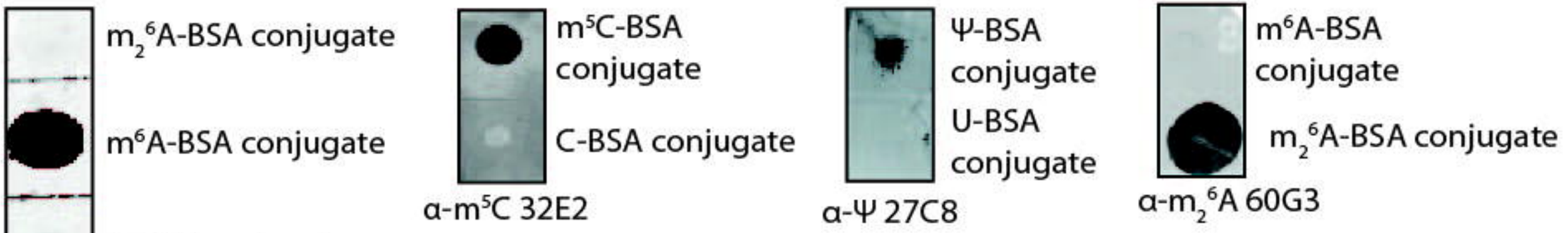
m2 6A-BSA conjugate
m6A-BSA conjugate
A-BSA conjugate
α-m6A 9B7
m5C-BSA conjugate
C-BSA conjugate
α-m5C 32E2
Ψ-BSA conjugate
U-BSA conjugate
α-Ψ 27C8
m6A-BSA conjugate
m2 6A-BSA conjugate
α-m2 6A 60G3

C

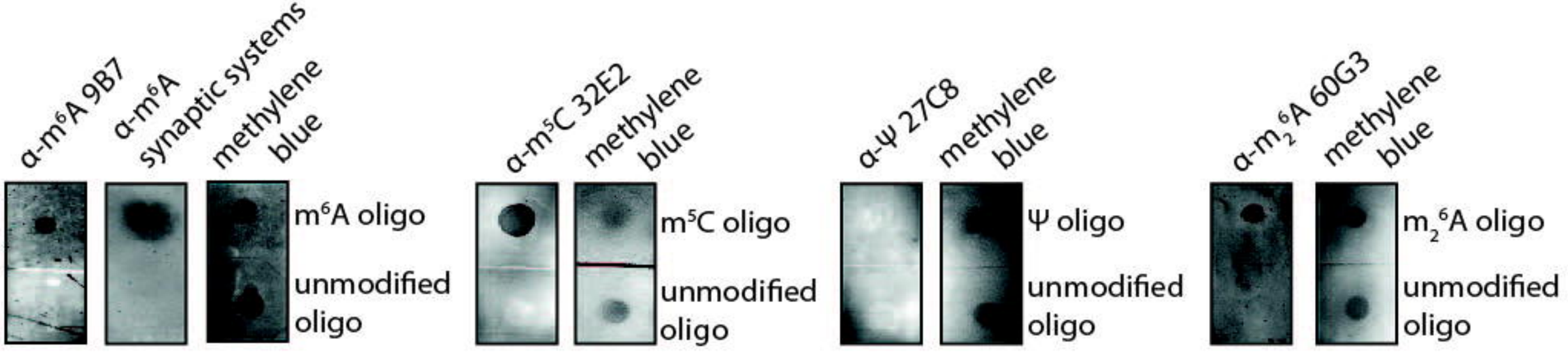
α-m6A 9B7
α-m6A synaptic systems
methylene blue
m6A oligo
unmodified oligo
α-m5C 32E2
methylene blue
m5C oligo
unmodified oligo
α-Ψ 27C8
methylene blue
Ψ oligo
unmodified oligo
α-m2 6A 60G3
methylene blue
m2 6A oligo
unmodified oligo

Figure 4

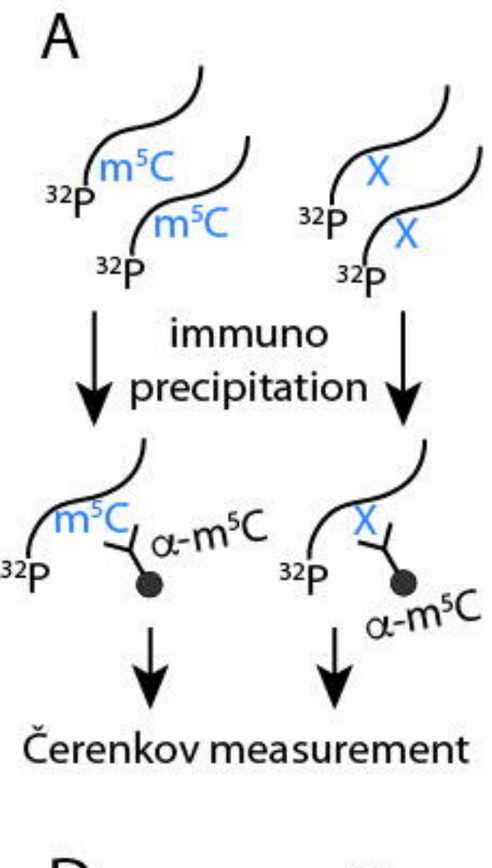
A
m5C
32P
m5C
32P
X
32P
X
32P
immuno
precipitation
m5C
α-m5C
32P
X
32P
α-m5C
Čerenkov measurement

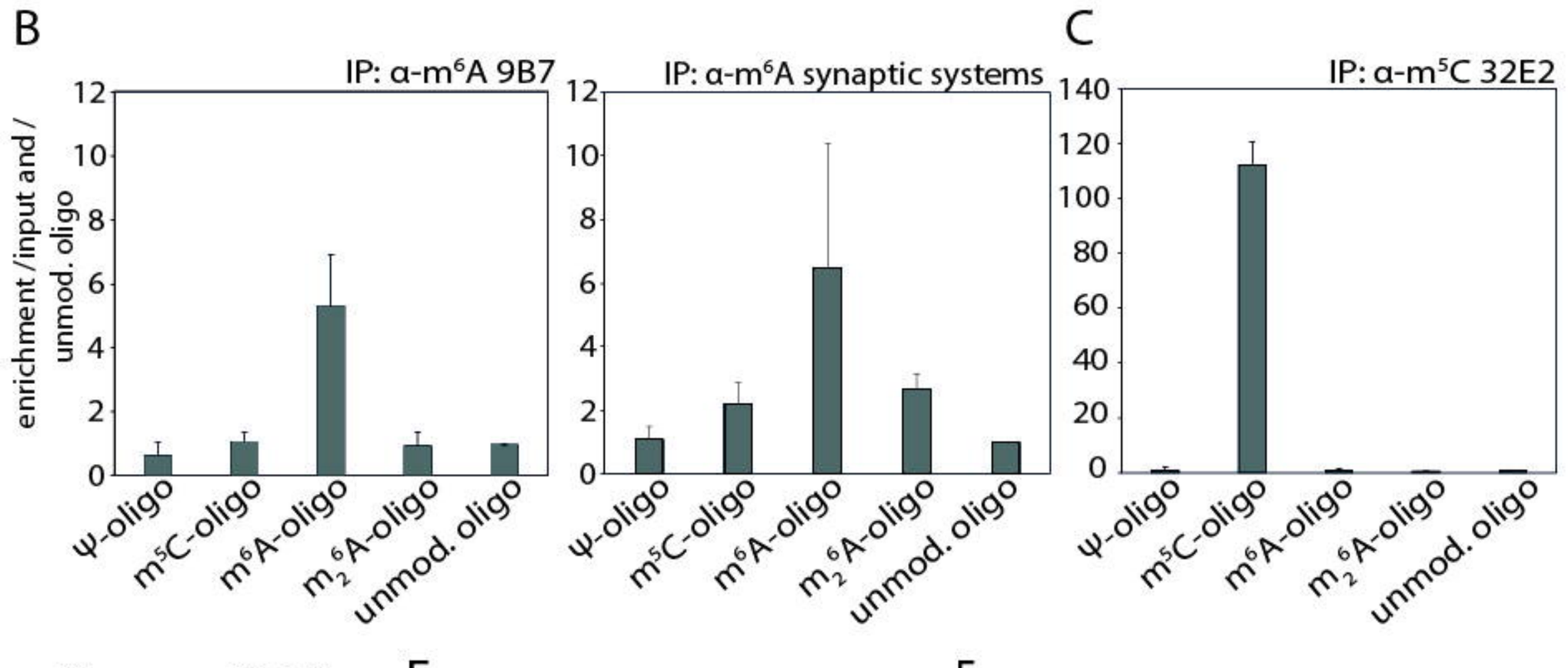
B
IP: α-m6A 9B7
IP: α-m6A synaptic systems
enrichment /input and / unmod. oligo
0
2
4
6
8
10
12
Ψ-oligo
m5C-oligo
m6A-oligo
m2 6A-oligo
unmod. oligo
C
IP: α-m5C 32E2
0
20
40
60
80
100
120
140

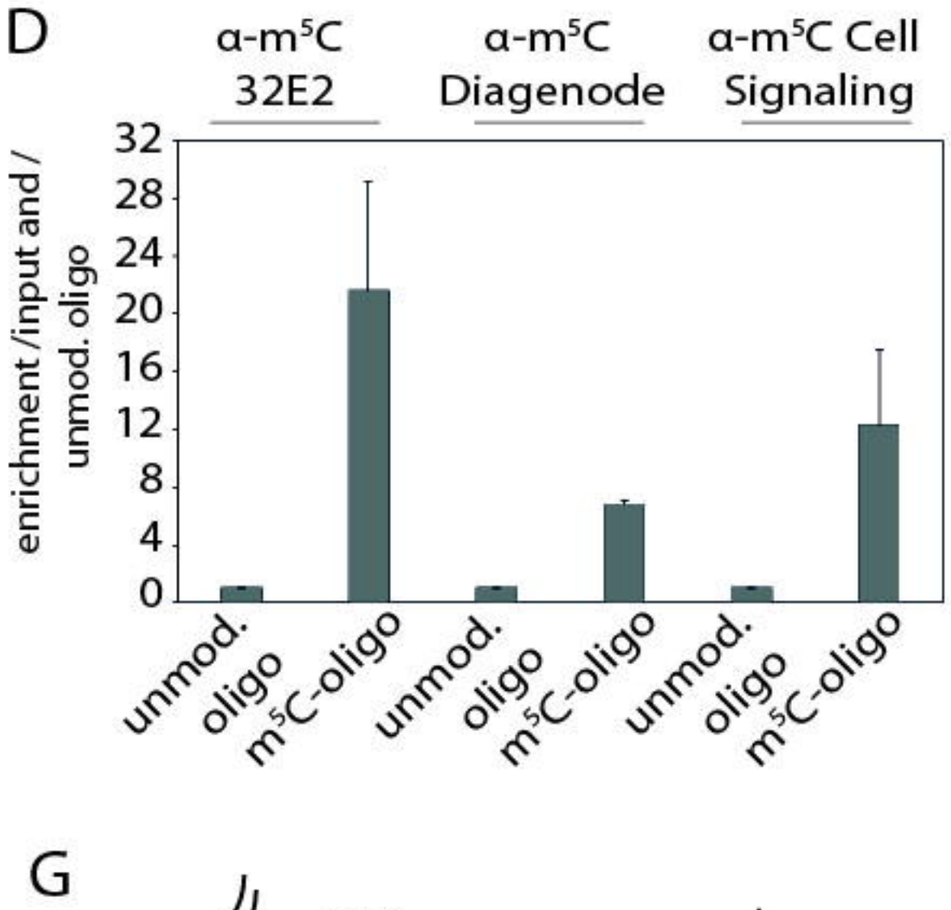
D
α-m5C
32E2
α-m5C
Diagenode
α-m5C Cell
Signaling
enrichment /input and / unmod. oligo
0
4
8
12
16
20
24
28
32
unmod. oligo
m5C-oligo

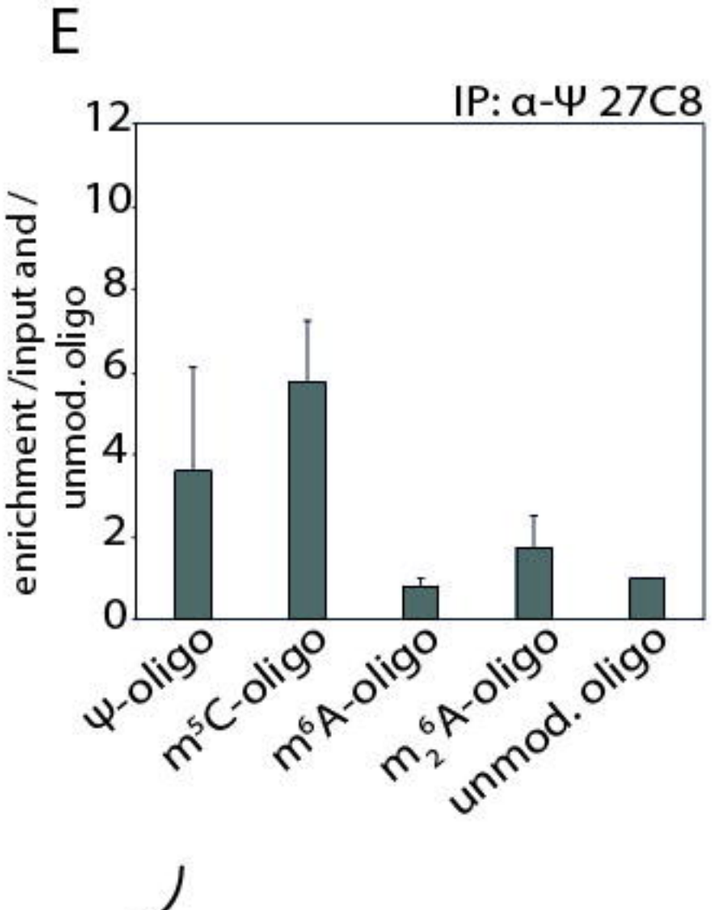
E
IP: α-Ψ 27C8
enrichment /input and / unmod. oligo
0
2
4
6
8
10
12
Ψ-oligo
m5C-oligo
m6A-oligo
m2 6A-oligo
unmod. oligo

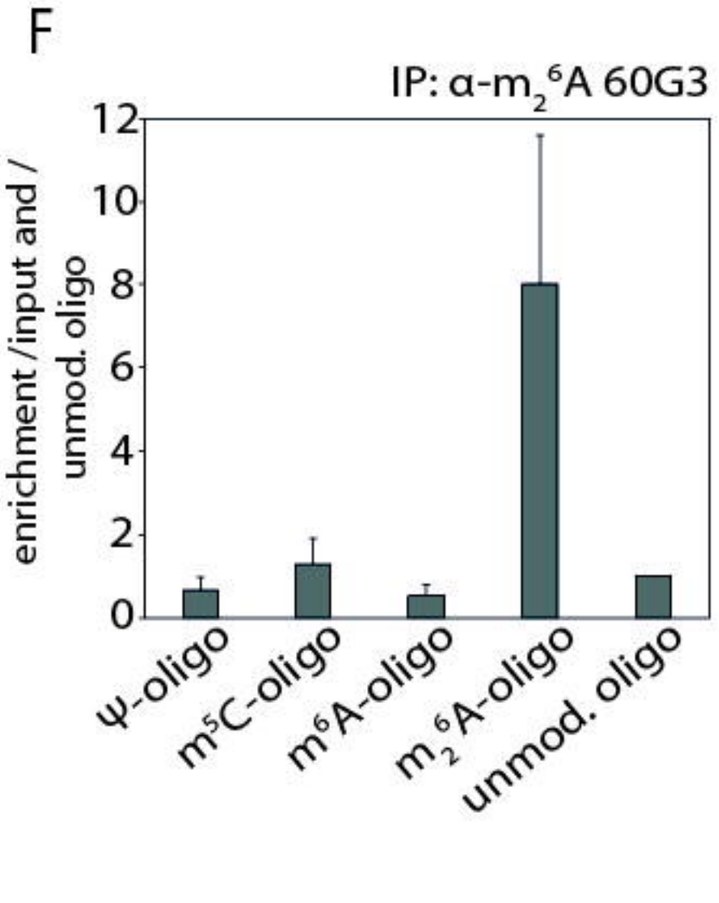
F
IP: α-m2 6A 60G3
enrichment /input and / unmod. oligo
0
2
4
6
8
10
12
Ψ-oligo
m5C-oligo
m6A-oligo
m2 6A-oligo
unmod. oligo

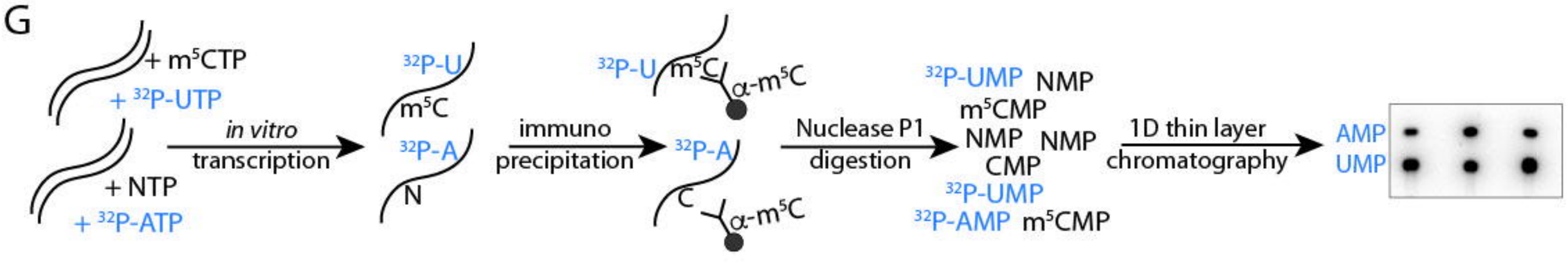
G
+ m5CTP
+ 32P-UTP
+ NTP
+ 32P-ATP
in vitro
transcription
32P-U
m5C
32P-A
N
immuno
precipitation
32P-U
m5C
α-m5C
32P-A
C
α-m5C
Nuclease P1
digestion
32P-UMP
NMP
m5CMP
NMP
NMP
CMP
32P-UMP
32P-AMP
m5CMP
1D thin layer
chromatography
AMP
UMP

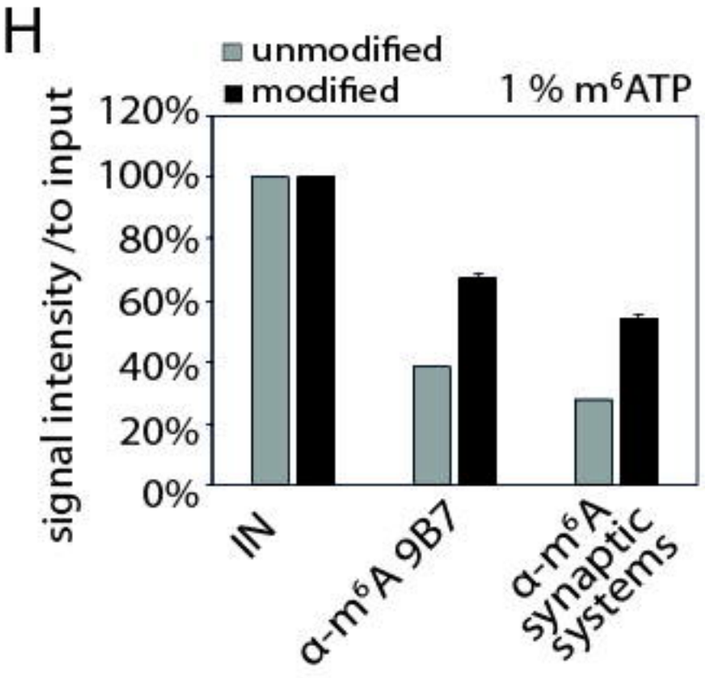
H
unmodified
modified
1 % m6ATP
signal intensity /to input
0%
20%
40%
60%
80%
100%
120%
IN
α-m6A 9B7
α-m6A synaptic systems

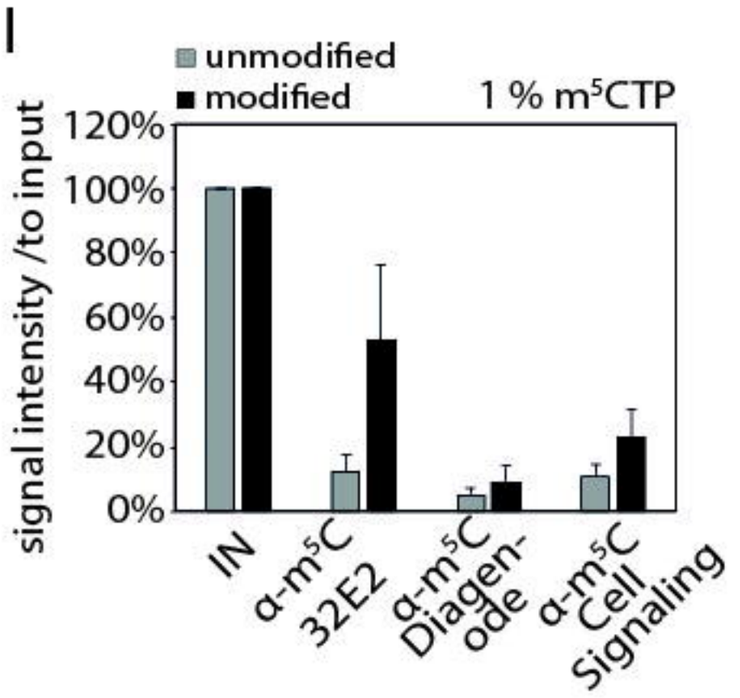
I
unmodified
modified
1 % m5CTP
signal intensity /to input
0%
20%
40%
60%
80%
100%
120%
IN
α-m5C 32E2
α-m5C Diagen-ode
α-m5C Cell Signaling

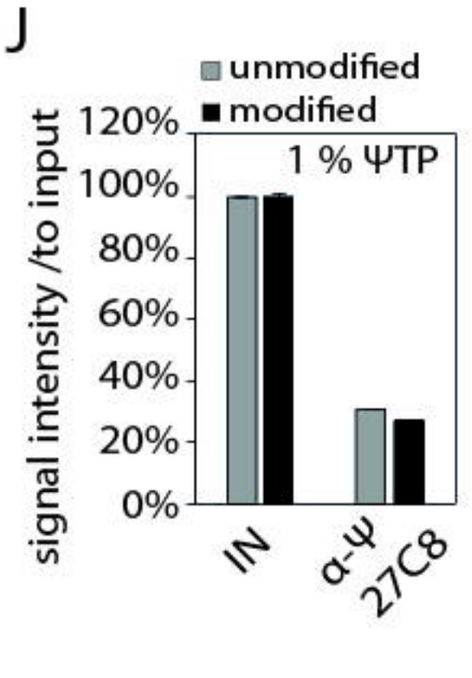
J
unmodified
modified
1 % ΨTP
signal intensity /to input
0%
20%
40%
60%
80%
100%
120%
IN
α-Ψ 27C8

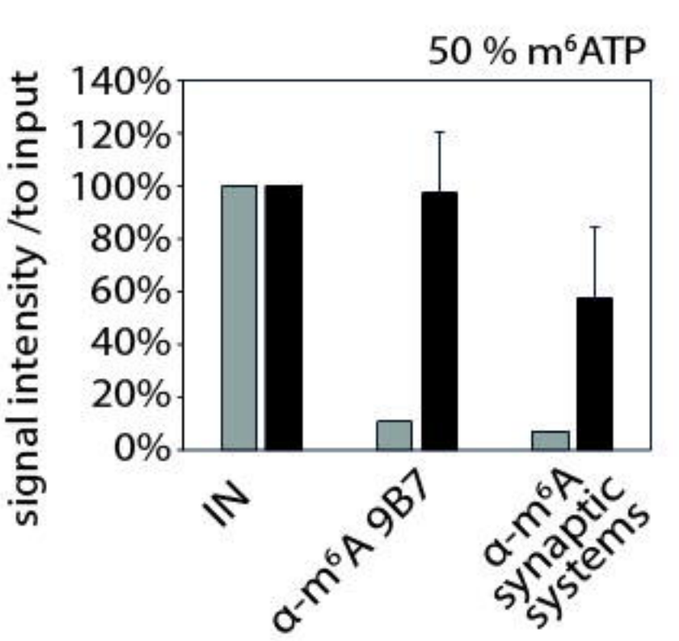
50 % m6ATP
signal intensity /to input
0%
20%
40%
60%
80%
100%
120%
140%
IN
α-m6A 9B7
α-m6A synaptic systems

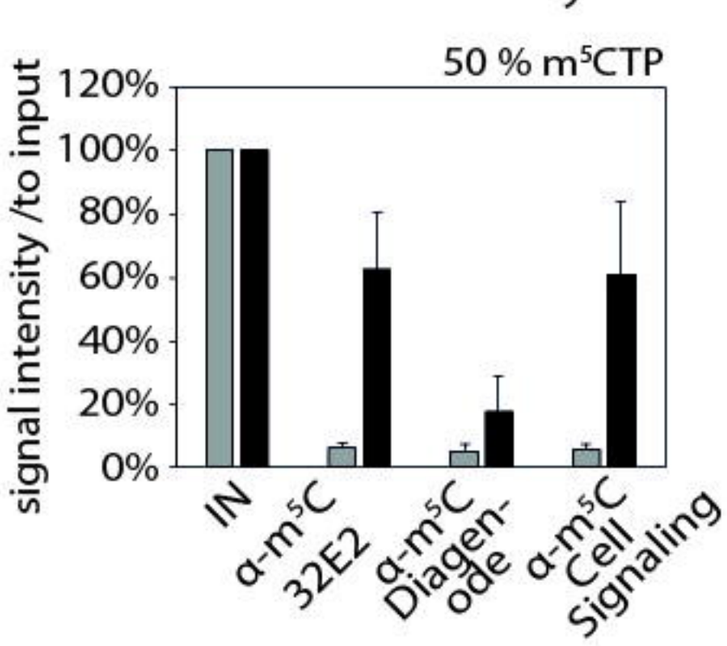
50 % m5CTP
signal intensity /to input
0%
20%
40%
60%
80%
100%
120%
IN
α-m5C 32E2
α-m5C Diagen-ode
α-m5C Cell Signaling

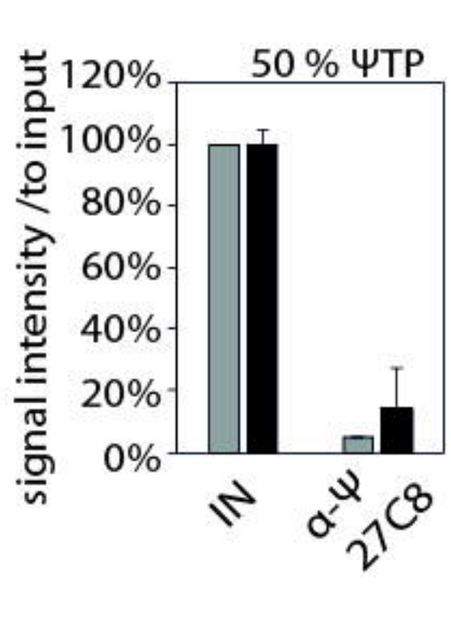
50 % ΨTP
signal intensity /to input
0%
20%
40%
60%
80%
100%
120%
IN
α-Ψ 27C8

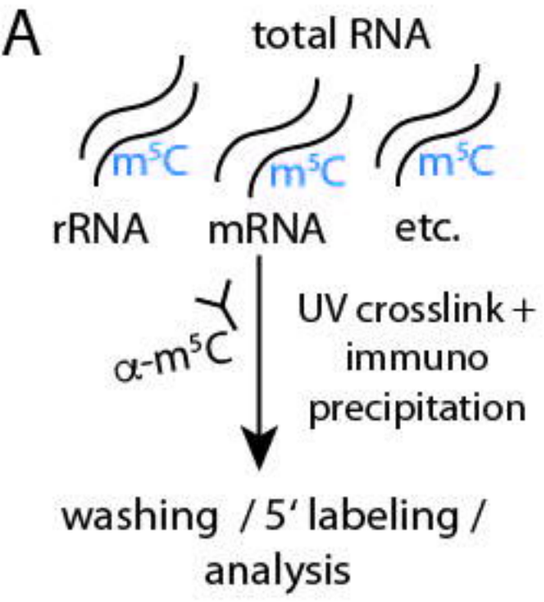
A
total RNA
m5C
rRNA
mRNA
etc.
α-m5C
UV crosslink + immuno precipitation
washing / 5' labeling / analysis

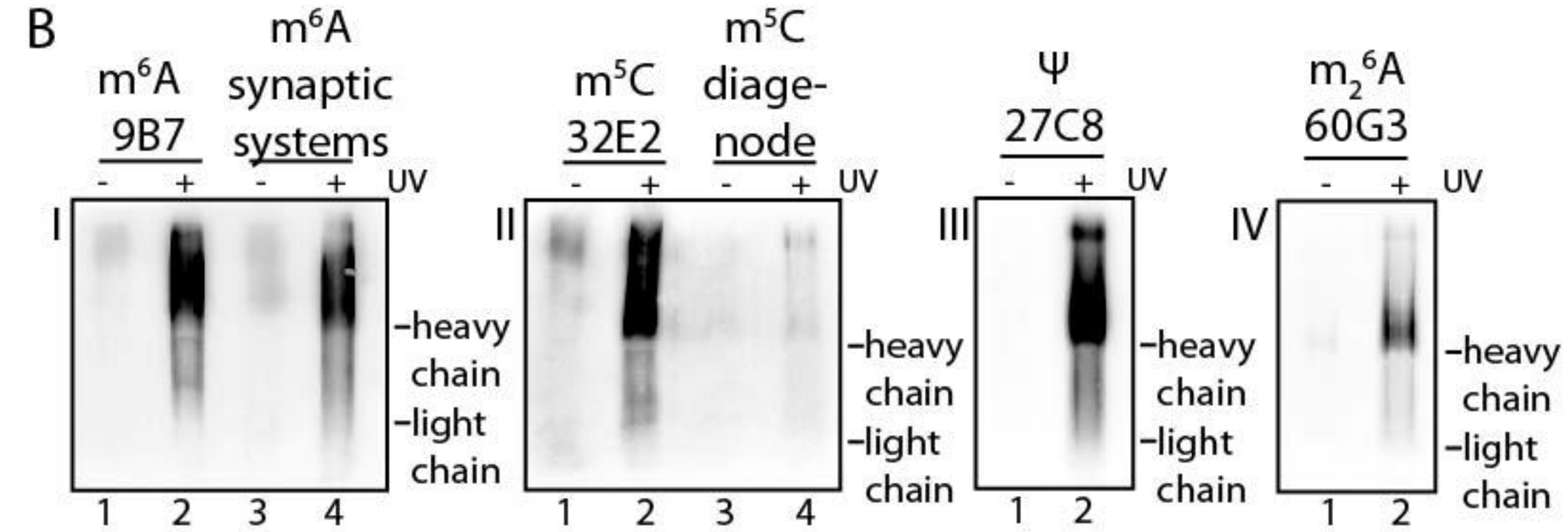
B
m6A 9B7
m6A synaptic systems
m5C 32E2
m5C diage-node
Ψ 27C8
m2 6A 60G3
- + - + UV
I
II
III
IV
-heavy chain
-light chain
1 2 3 4

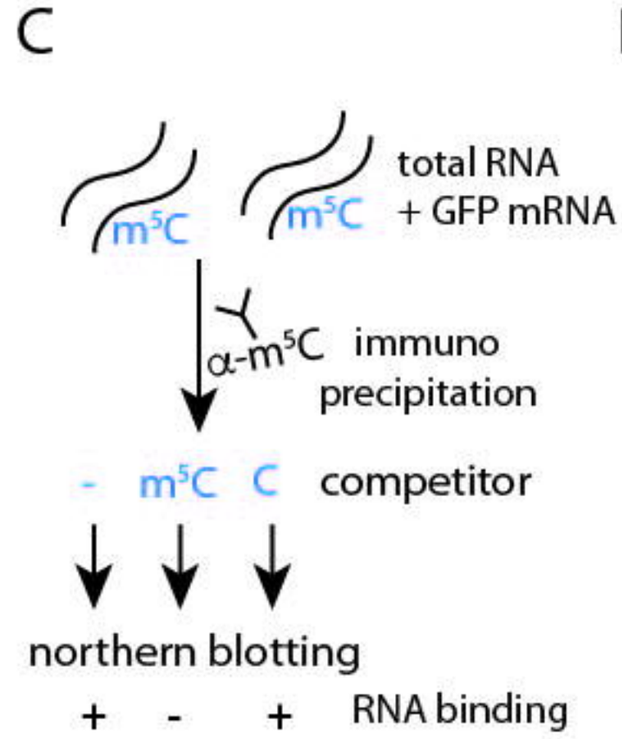
C
total RNA + GFP mRNA
m5C
α-m5C immuno precipitation
- m5C C competitor
northern blotting
+ - + RNA binding

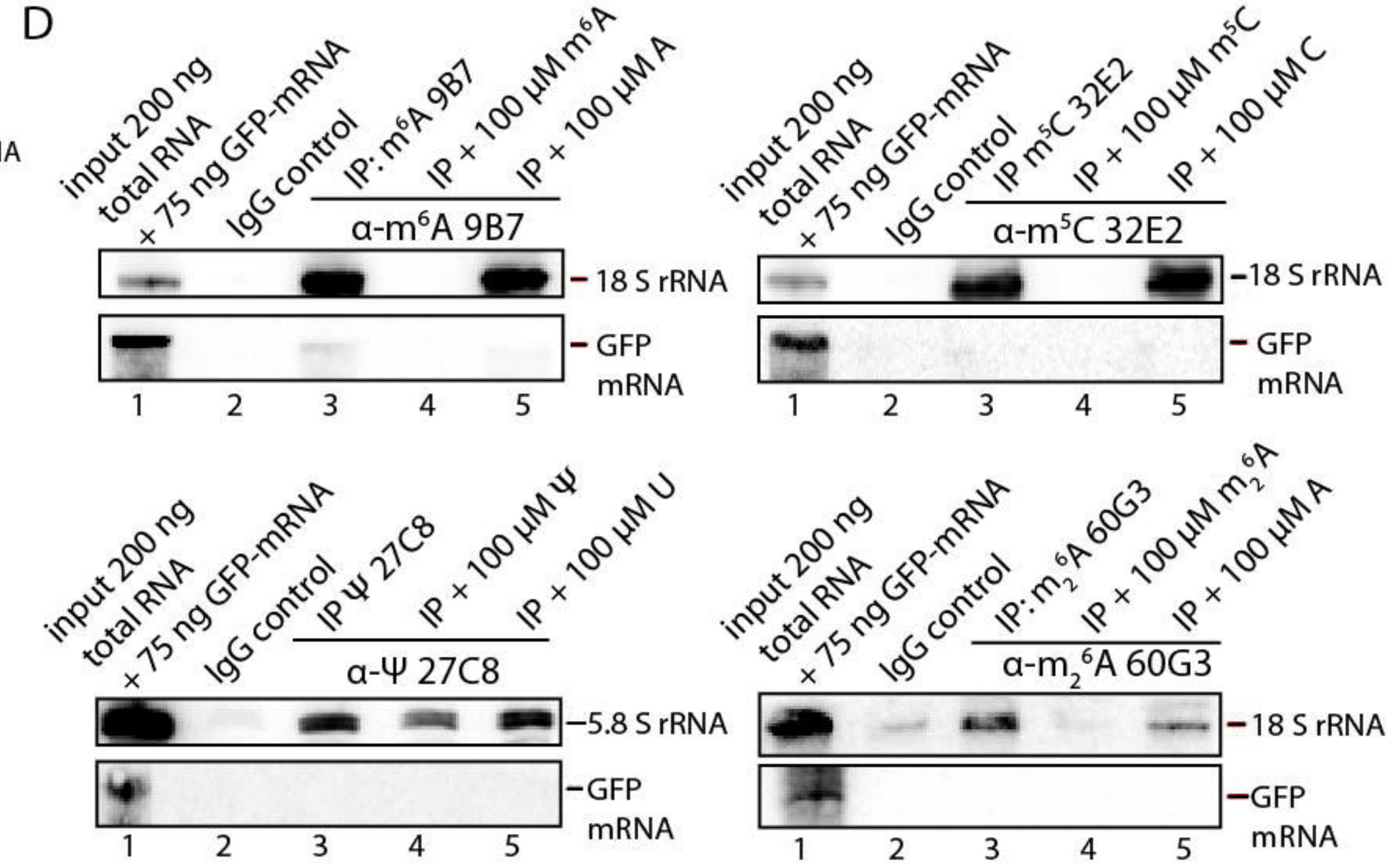
D
input 200 ng total RNA + 75 ng GFP-mRNA
IgG control
IP: m6A 9B7
IP + 100 µM m6A
IP + 100 µM A
α-m6A 9B7
IP m5C 32E2
IP + 100 µM m5C
IP + 100 µM C
α-m5C 32E2
IP Ψ 27C8
IP + 100 µM Ψ
IP + 100 µM U
α-Ψ 27C8
IP: m2 6A 60G3
IP + 100 µM m2 6A
IP + 100 µM A
α-m2 6A 60G3
18 S rRNA
GFP mRNA
5.8 S rRNA
1 2 3 4 5

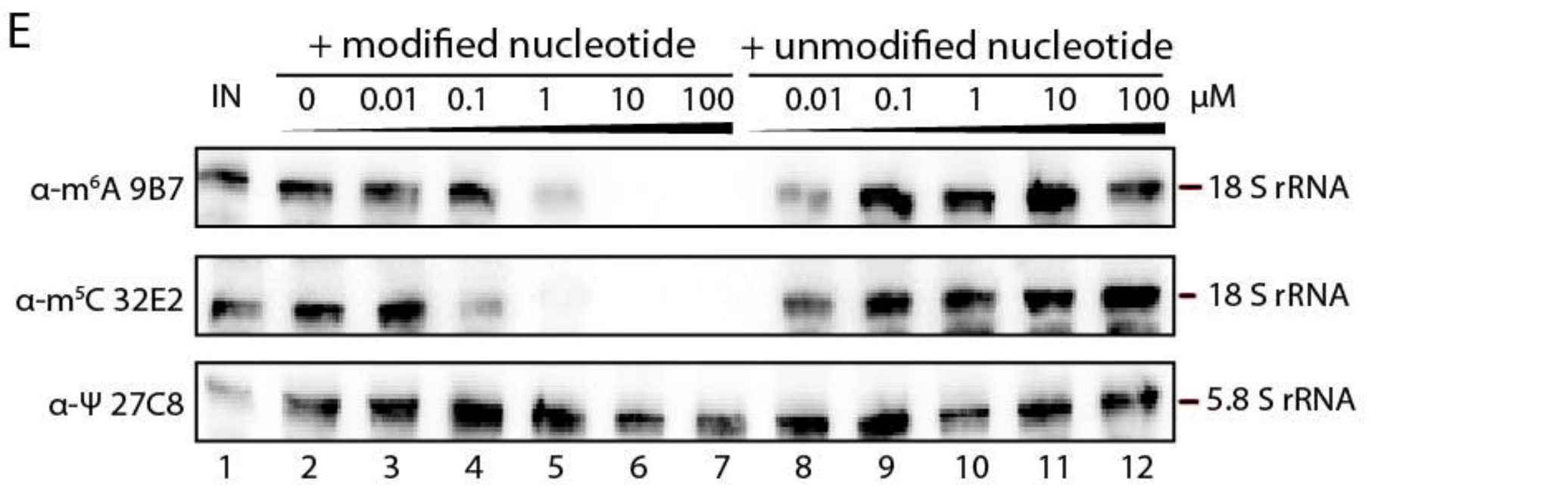
E
+ modified nucleotide
+ unmodified nucleotide
IN
0 0.01 0.1 1 10 100 0.01 0.1 1 10 100 µM
α-m6A 9B7
α-m5C 32E2
α-Ψ 27C8
18 S rRNA
18 S rRNA
5.8 S rRNA
1 2 3 4 5 6 7 8 9 10 11 12

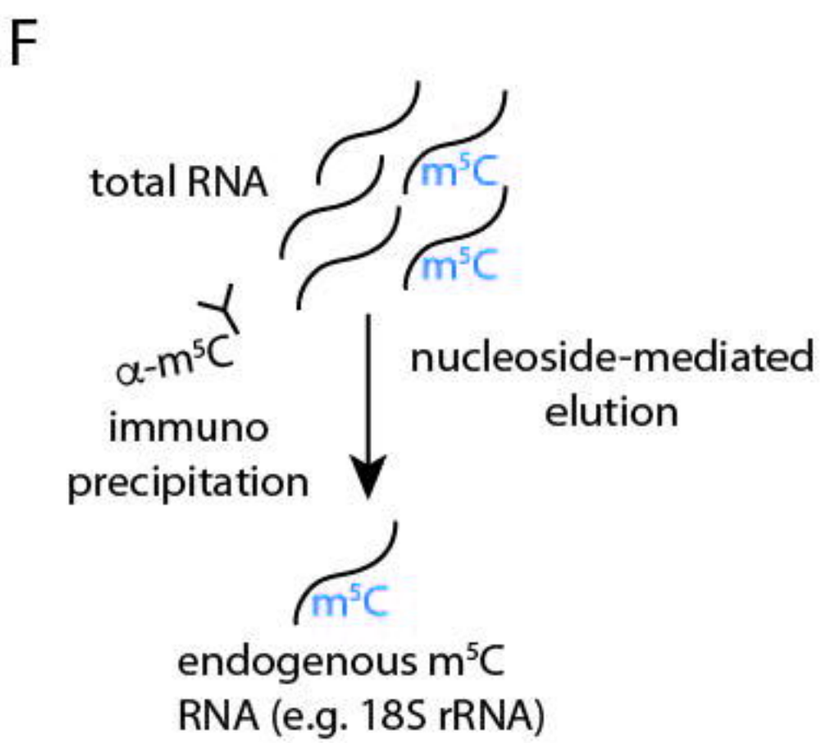
F
total RNA
m5C
α-m5C
immuno precipitation
nucleoside-mediated elution
m5C
endogenous m5C RNA (e.g. 18S rRNA)

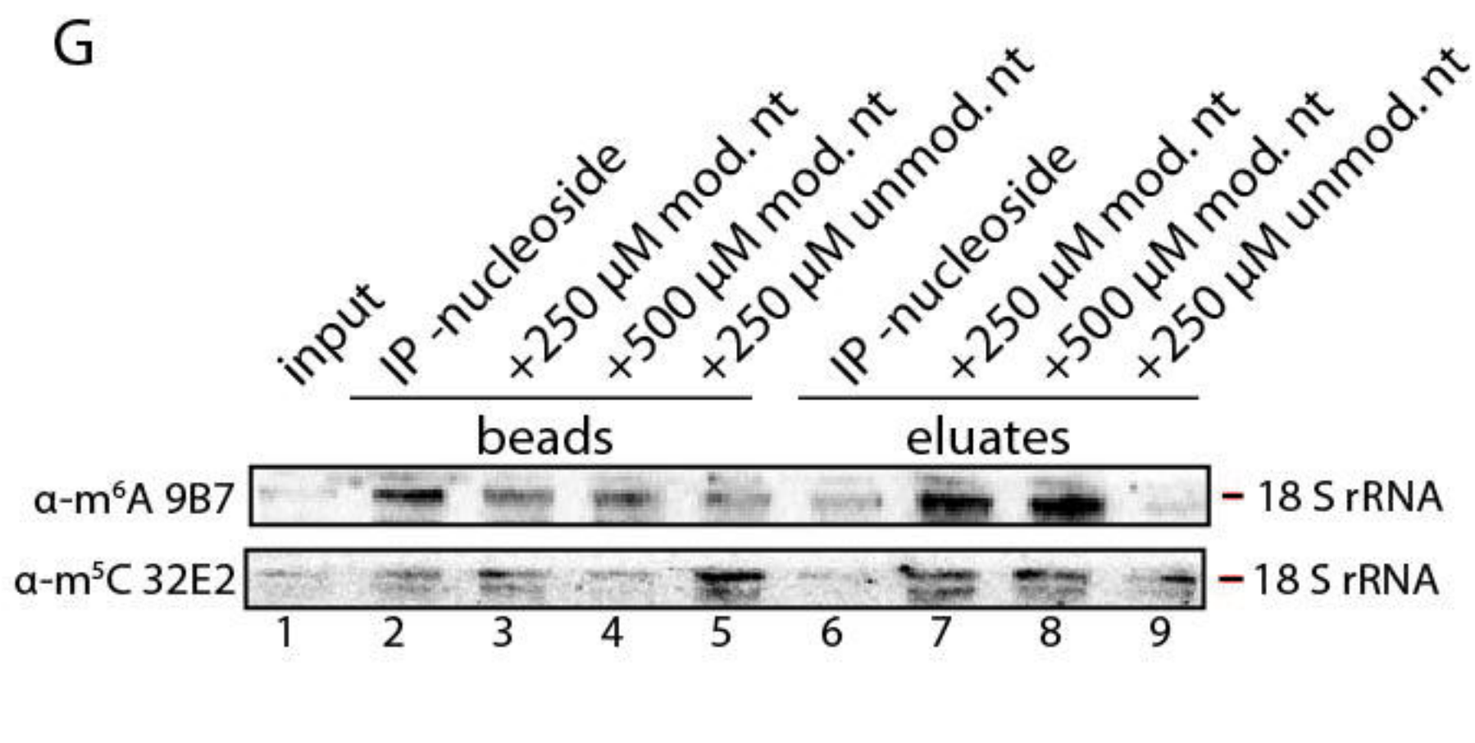
G
input
IP -nucleoside
+250 µM mod. nt
+500 µM mod. nt
+250 µM unmod. nt
beads
eluates
α-m6A 9B7
α-m5C 32E2
18 S rRNA
18 S rRNA
1 2 3 4 5 6 7 8 9

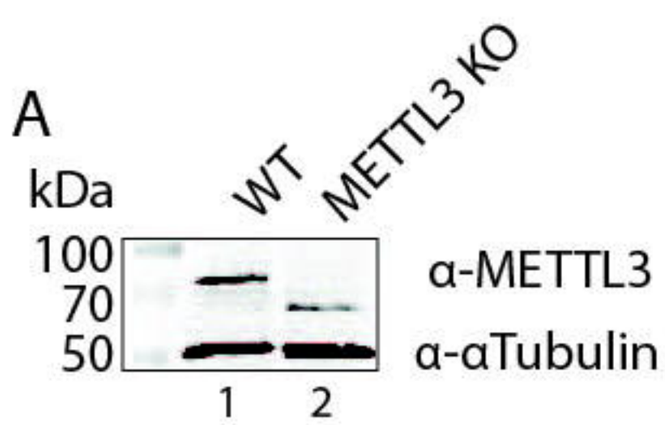
A
kDa
WT
METTL3 KO
100
70
50
α-METTL3
α-αTubulin
1
2

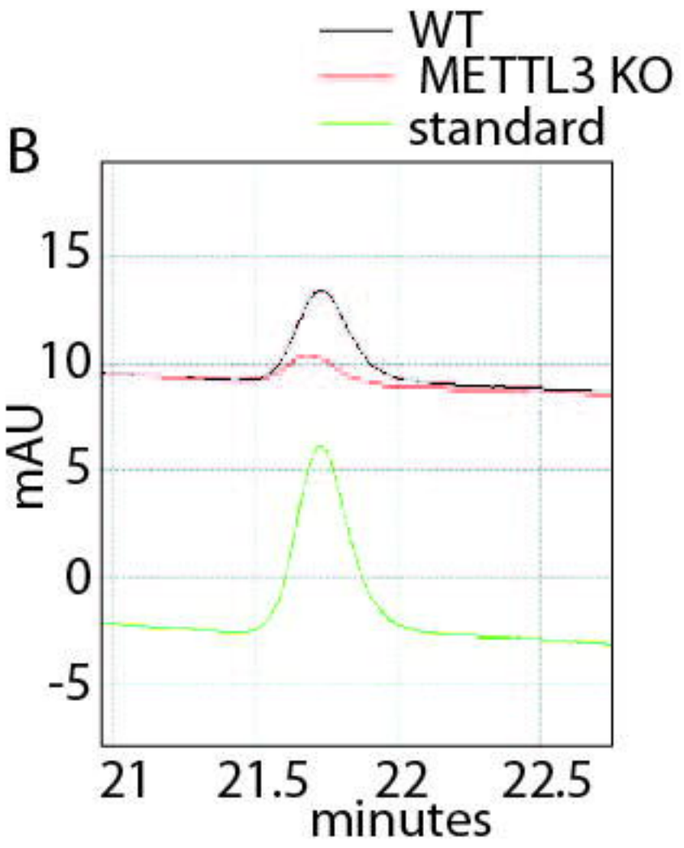
B
WT
METTL3 KO
standard
mAU
15
10
5
0
-5
21
21.5
22
22.5
minutes

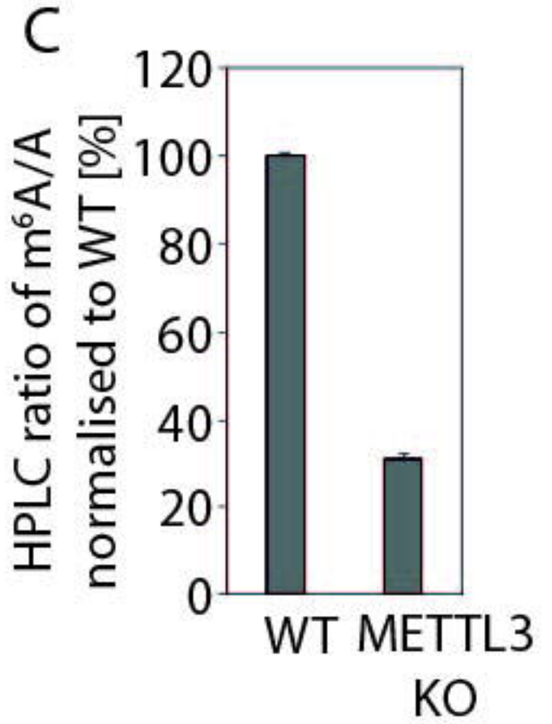
C
HPLC ratio of m⁶A/A normalised to WT [%]
120
100
80
60
40
20
0
WT
METTL3 KO

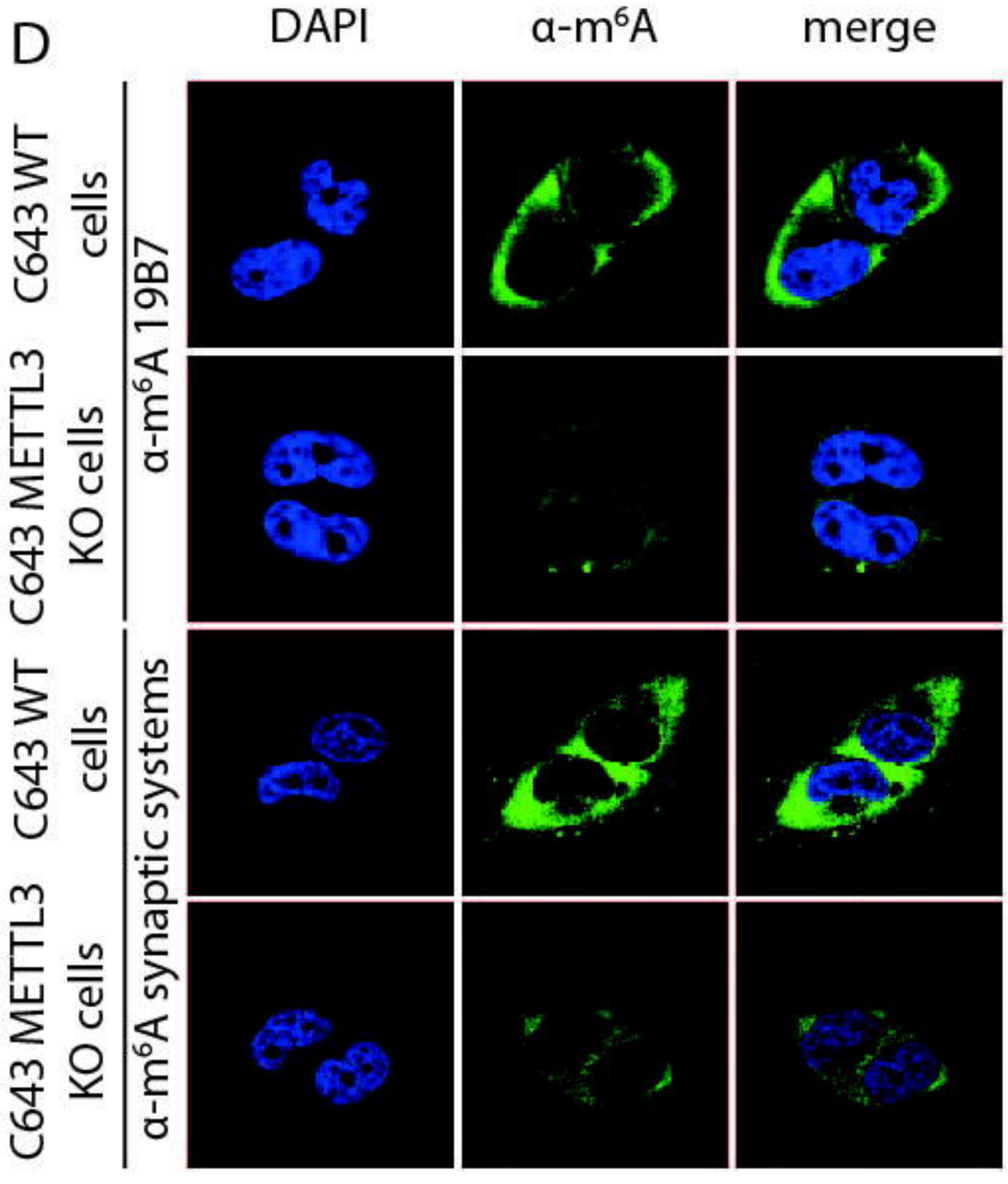
D
DAPI
α-m⁶A
merge
C643 WT cells
C643 METTL3 KO cells
α-m⁶A 19B7
C643 WT cells
C643 METTL3 KO cells
α-m⁶A synaptic systems

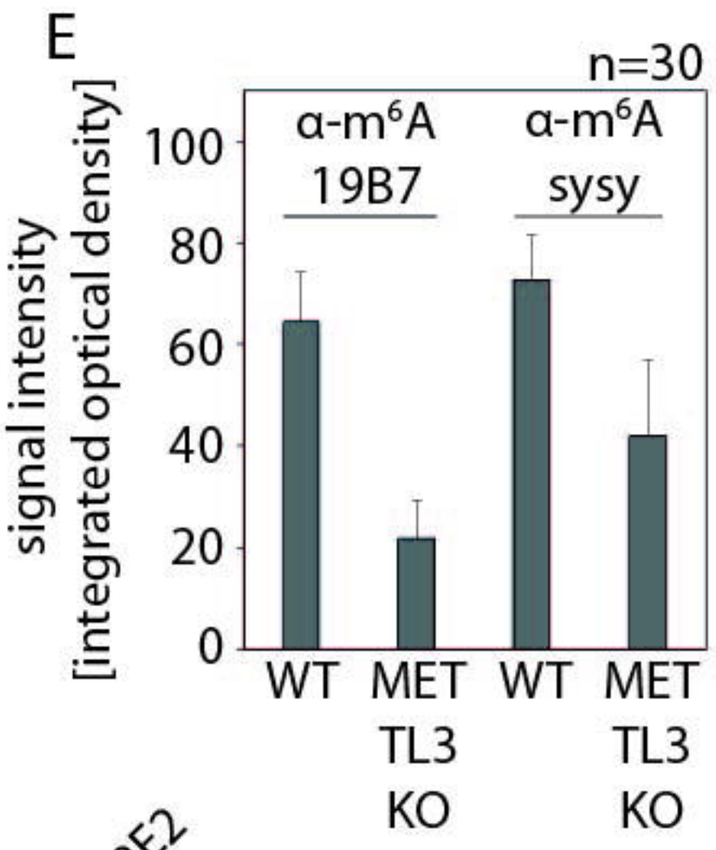
E
n=30
α-m⁶A 19B7
α-m⁶A sysy
signal intensity [integrated optical density]
100
80
60
40
20
0
WT
MET TL3 KO
WT
MET TL3 KO

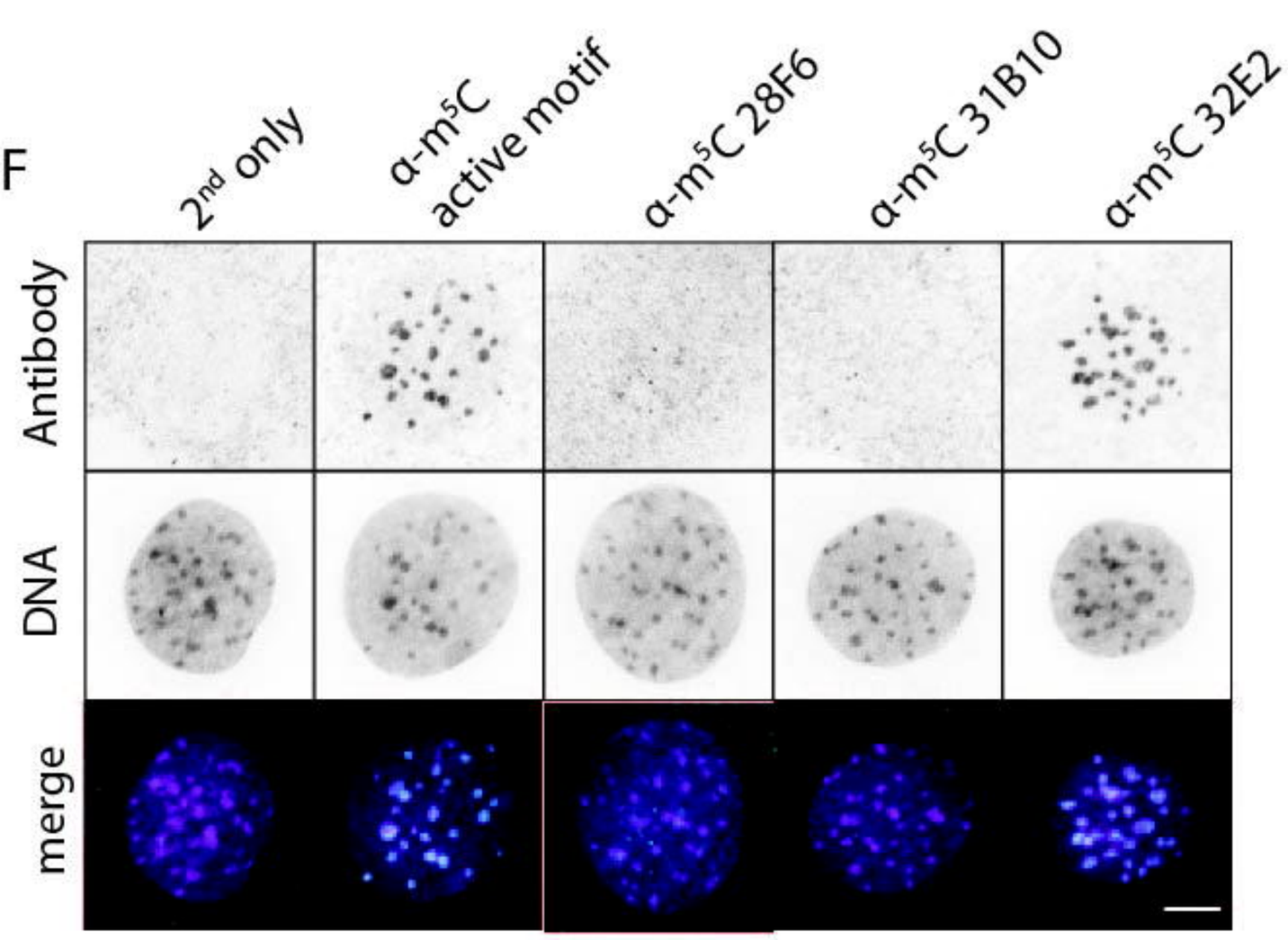
F
2nd only
α-m⁵C active motif
α-m⁵C 28F6
α-m⁵C 31B10
α-m⁵C 32E2
Antibody
DNA
merge

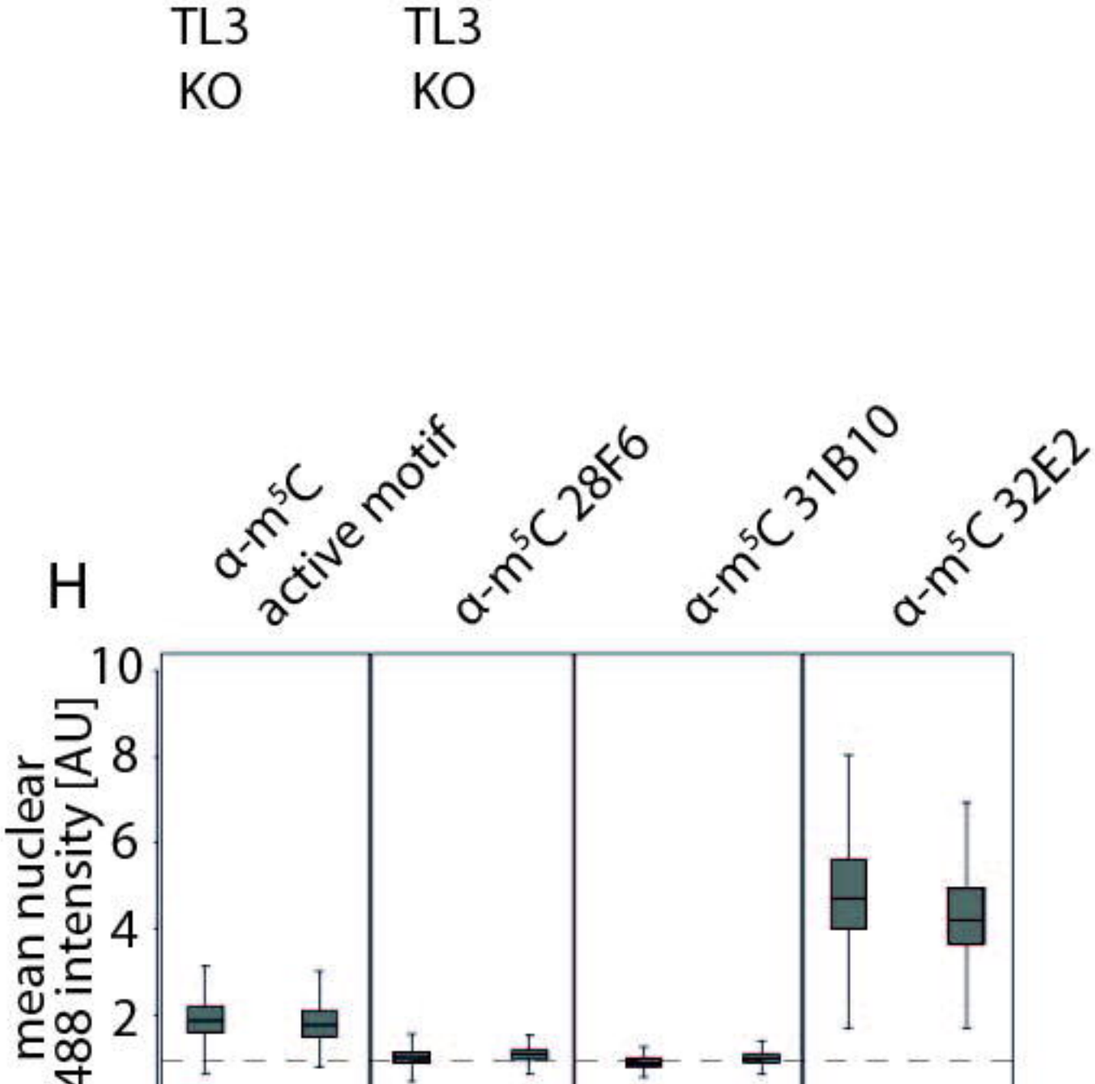
H
α-m⁵C active motif
α-m⁵C 28F6
α-m⁵C 31B10
α-m⁵C 32E2
mean nuclear 488 intensity [AU]
10
8
6
4
2
0
RNaseA - + - + - + - +

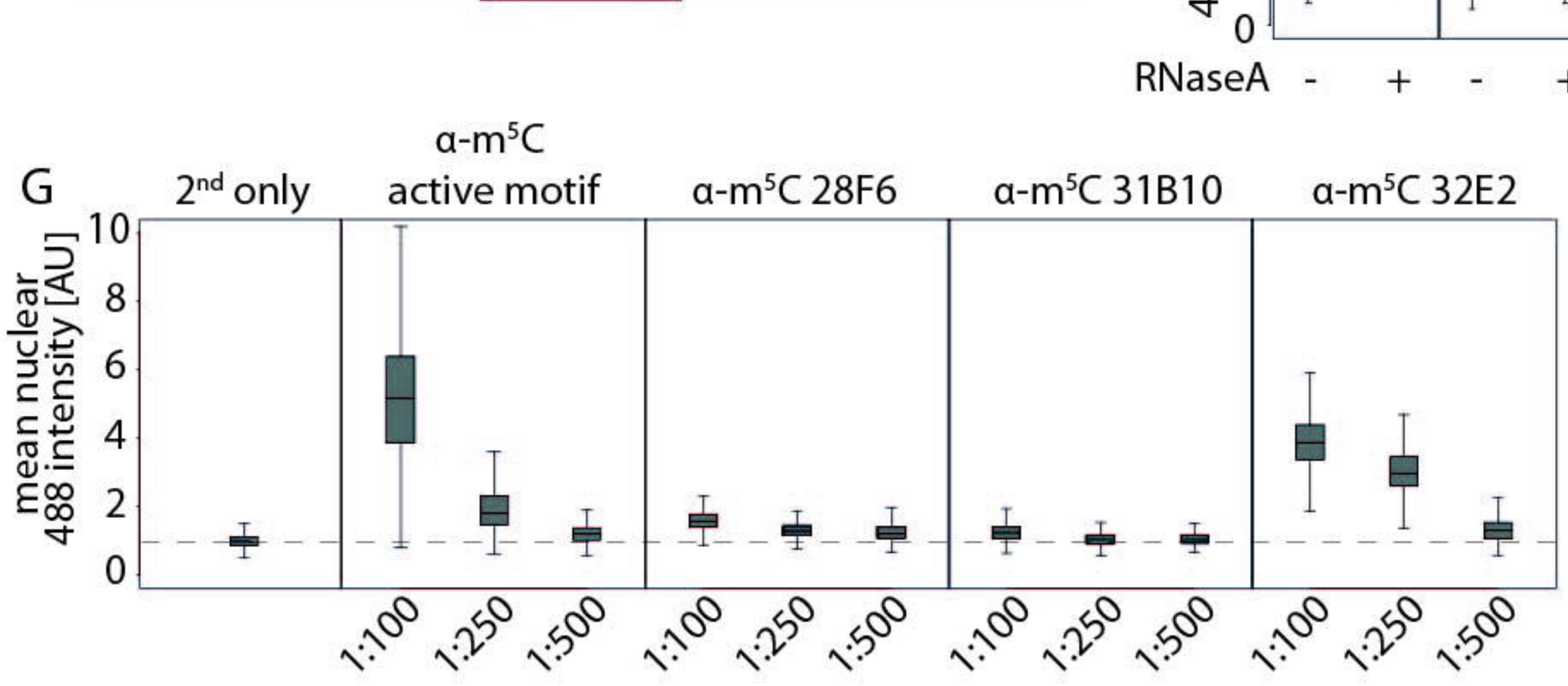
G
2nd only
α-m⁵C active motif
α-m⁵C 28F6
α-m⁵C 31B10
α-m⁵C 32E2
mean nuclear 488 intensity [AU]
10
8
6
4
2
0
1:100
1:250
1:500

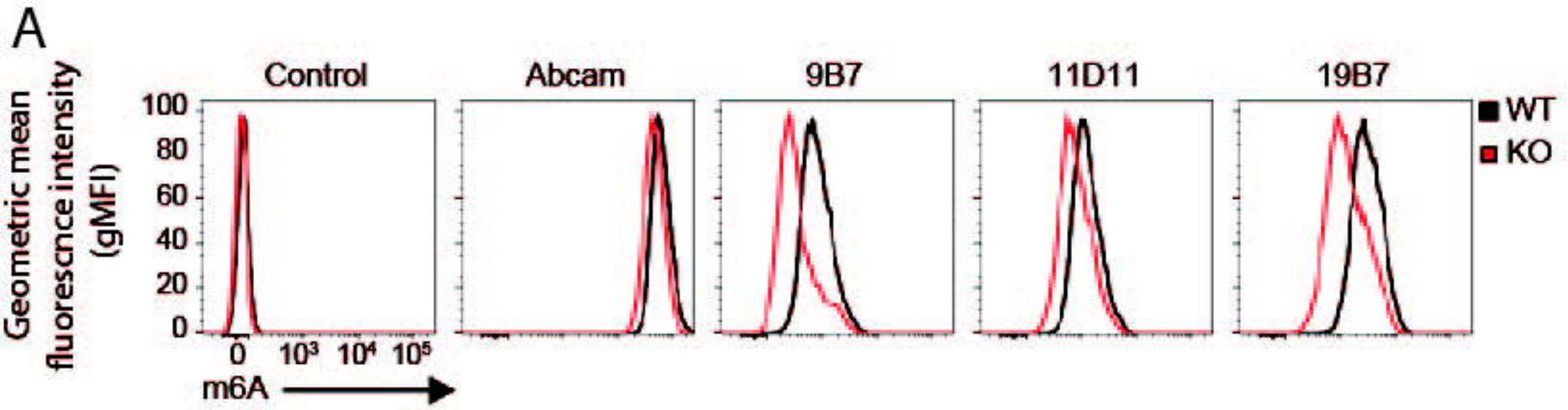
A
Control
Abcam
9B7
11D11
19B7
Geometric mean fluorescnce intensity (gMFI)
100
80
60
40
20
0
0
10³
10⁴
10⁵
m6A
WT
KO

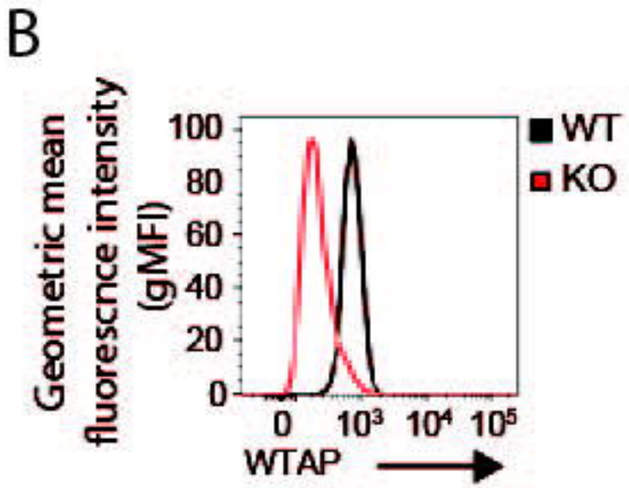
B
Geometric mean fluorescnce intensity (gMFI)
100
80
60
40
20
0
0
10³
10⁴
10⁵
WTAP
WT
KO

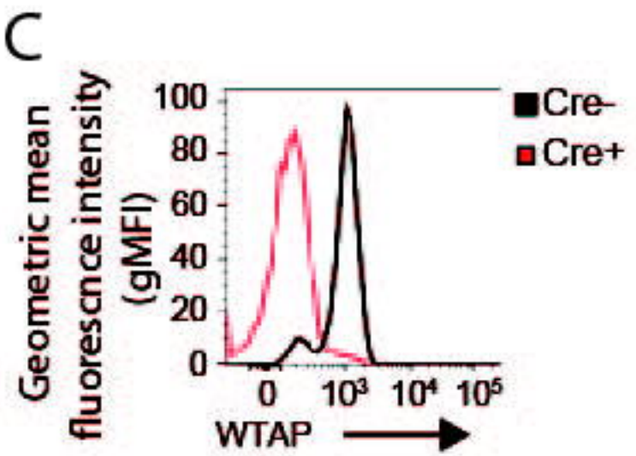
C
Geometric mean fluorescnce intensity (gMFI)
100
80
60
40
20
0
0
10³
10⁴
10⁵
WTAP
Cre-
Cre+

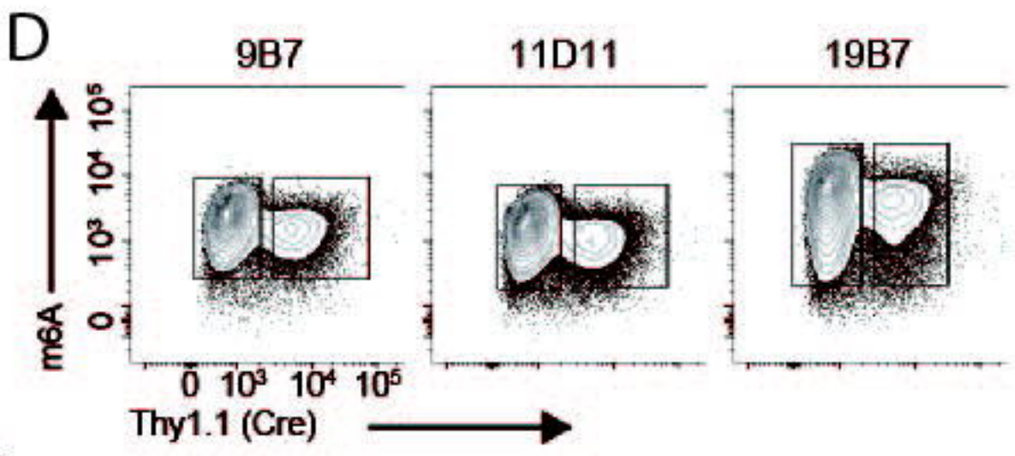
D
9B7
11D11
19B7
m6A
0
10³
10⁴
10⁵
Thy1.1 (Cre)

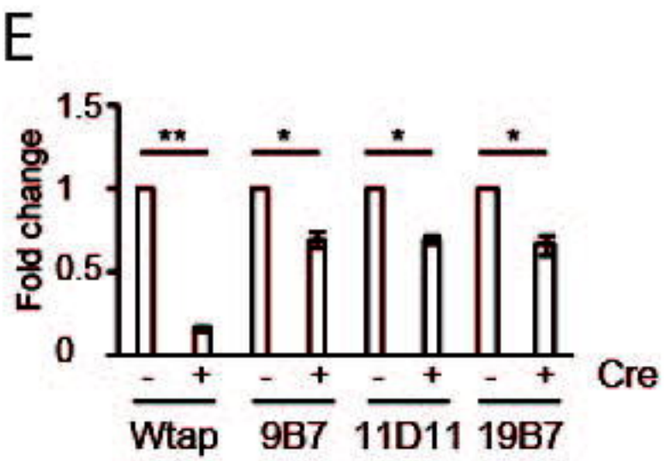
E
Fold change
1.5
1
0.5
0
**
*
*
*
-
+
-
+
-
+
-
+
Cre
Wtap
9B7
11D11
19B7

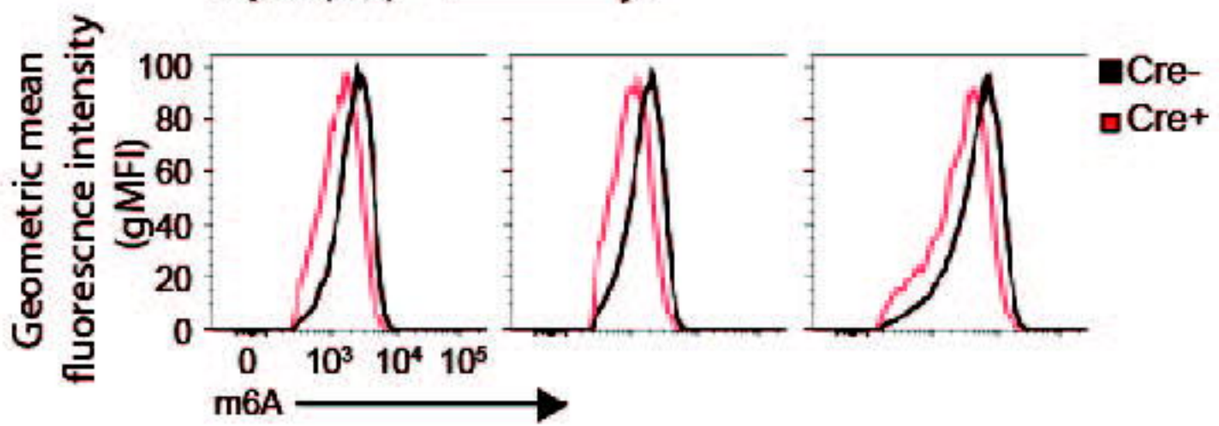
Geometric mean fluorescnce intensity (gMFI)
100
80
60
40
20
0
0
10³
10⁴
10⁵
m6A
Cre-
Cre+